Journal of Hazardous Materials 421 (2022) 126657

Contents lists available at ScienceDirect

Journal of Hazardous Materials

journal homepage: www.elsevier.com/locate/jhazmat

Research Paper

Adsorption and recovery of lithium ions from groundwater using date pits impregnated with cellulose nanocrystals and ionic liquid

Sara A. Wahib [a], Dana A. Da'na [a], Nabil Zaouri [a], Yousef M. Hijji [b], Mohammad A. Al-Ghouti [a,*]

[a] Department of Biological and Environmental Sciences, College of Arts and Sciences, Qatar University, P.O. Box: 2713, Doha, Qatar
[b] Department of Chemistry and Earth Sciences, College of Arts and Sciences, Qatar University, P.O. Box 2713, Doha, Qatar

ARTICLE INFO

Editor: Dr. H. Artuto

Keywords:
Agricultural wastes
Cellulose extraction
Cellulose nanocrystals
Ionic liquid, Bio-based nanoscale products

ABSTRACT

The study aims to prepare a novel low-cost and environmentally friendly adsorbent by using date pits (DP) impregnated with cellulose nanocrystals (CNCs) and ionic liquid (IL), named IL-CNC@DP. The batch adsorption of lithium onto IL-CNC@DP and DP were studied at different pH values, initial lithium concentrations, and temperatures. The thermodynamics constants of the adsorption process showed that the IL-CNC@DP was exothermic, did not favor a high level of disorder, and spontaneous in nature. At pH 6, there is a significant increase in the removal efficiency where it increased to 90%. This also could be explained by the fact that electrostatic attraction forces and hydrogen bonding existed between the protonated Li^+ and the less protonated IL-CNC@DP adsorbent surface, which enhanced the percentage of Li^+ removal. A strong inter- and intra-hydrogen bonding (O-H) stretching absorption is seen at 3311 cm^{-1} that occurs in cellulose components. In conclusion, the IL-CNC@DP in comparison to the DP confirmed exceptional results proving that the modification enhanced the remediation of the Li^+ from water. Furthermore, the selectivity of IL-CNC@DP towards real groundwater samples isolated in Qatar depends upon the physicochemical characteristics of each element.

1. Introduction

In Qatar, two types of natural renewable resources exist, namely groundwater and rainfall. Yet, the challenge will arise when such resources begin depleting each year (Darwish and Mohtar, 2013). Moreover, the country is moving towards prosperity in terms of economic and industrial activities with the increase in resource consumption and population, hence water challenges be expected to occur. As a result, Qatar will become unsustainable as the demand for water will increase and this will lead to a national water crisis in the region (Hussein and Lambert, 2020). The low rates of precipitation are not enough to solve the issue with water demand; therefore, Qatar can rely on groundwater aquifers as the sole source of renewable water resources (Baalousha and Ouda, 2017; Ismail, 2015). This will lead to overexploitation of the groundwater that can decrease and deteriorate the quality of the water. Several contaminants including toxic metals and metalloids may introduce in the water systems that could exceed permissible limits. For example, lithium (Li) was found to be 0.120 mg/L as a mean value for 41 wells in Qatar's groundwater aquifers (Ahmad et al., 2020). The lithium concentration was ranged from 0.02334 mg/L to 0.2367 mg/L. Table 1 presents some commonly found cations in groundwater and their permissible concentrations according to guidelines and standards.

Lithium is of great concern as it can potentially induce toxicity to agricultural products if they exceed permissible levels (Shi et al., 2018). Moreover, since groundwater in Qatar is used for agricultural purposes, then this will greatly impact human consumption (Hussein and Lambert, 2020). Hence, investigating the adsorption mechanism of lithium on the surface of different adsorbents could lead to the development of an effective lithium separation method (Wiśniewska et al., 2020). As a result, the development of low-cost treatment technology, such as adsorption, that is able to treat and reuse groundwater for food production is the main purpose of this study.

Adsorption is considered a widely promising remediation technique used to treat wastewaters as a way to overcome the challenges that are associated with conventional and advanced water treatment methods. Due to its low cost, feasibility, environmentally friendly, and simple operation, adsorption is employed tremendously (Al-Ghouti and Al-Absi, 2020). Due to its excellent characteristics, adsorption methods were used on trace metals, dyes, and other pollutants. In particular, metals found in aquatic environments are a growing concern due to their

* Corresponding author.
E-mail address: mohammad.alghouti@qu.edu.qa (M.A. Al-Ghouti).

https://doi.org/10.1016/j.jhazmat.2021.126657
Received 30 March 2021; Received in revised form 27 June 2021; Accepted 13 July 2021
Available online 17 July 2021
0304-3894/© 2021 The Authors. Published by Elsevier B.V. This is an open access article under the CC BY license (http://creativecommons.org/licenses/by/4.0/).

toxicity and carcinogenicity (Wallace and Djordjevic, 2020). Factors like the effect of pH, initial concentration, temperature, and adsorption mechanisms tend to have an influence on the degree of remediation (Hawari et al., 2014; Wiśniewska et al., 2018a, 2018b). A commonly used low-cost adsorbent is date pits (Al-Ghouti et al., 2017, 2010). The source of these green adsorbents is generally based on locally available resources, which can be modified to enhance its sorption capacity (Pyrzynska et al., 2019). In this study, a cost-effective technique was developed using date pits (DP) as a locally available solid waste. Furthermore, nanomaterials possess a high surface area, which can be utilized to enhance adsorption capacity or removal efficiency. Hence, this study relies on conventional and well-tested acid hydrolysis techniques to convert extracted cellulose from date pits to cellulose nanocrystals (CNC) (Yongvanich, 2015; Morais et al., 2013).

Additionally, ionic liquids (ILs) are applied in many fields such as environmental sciences, chemistry (e.g. solvents, catalysts, reagents), chemical engineering (e.g. lubricants, liquid membranes, surfactants), biology, and pharmacy (e.g. biocides, drugs), electrochemistry (e.g. batteries, sensors), and other applications (e.g. polysaccharides, liquid crystals) (Verma et al., 2019). ILs possess unique properties in which they have high thermal stability, low vapor pressure, inflammability, and melting temperature, and viscosity that depends on the nature of anions. In this study, IL and CNC were used to functionalize the DP to create a modified adsorbent named IL-CNC@DP.

Zante et al. (2019) successfully demonstrated the use of supported ionic liquid membranes (SLMs) to extract lithium. The SLMs were used to separate lithium cations from a mixture of an aqueous solution by impregnating mixtures of hydrophobic ionic liquid. Impregnation of membranes shows that the mass uptake of ionic liquids is affiliated with the density of the organic phase. Moreover, the stability of the membrane is related to the solubility of the organic phase. As a result, due to the several useful features of ILs, they have been shown to combine with nanomaterials for combined functionalities and their use has been demonstrated in catalysis and separations. Another study reported that ILs could be applied to dissolve cellulose to fabricate cellulose nanofiber with gold nanoparticles as a hybrid. This hybrid could be later on used for the application of cellulose/gold nanoparticle sensors or the production of low-temperature catalysts (Li and Taubert, 2009). Adsorption of ILs is also applicable by using an adsorbent such as activated carbon. Hydrophobic ILs found in water streams can be adsorbed by modifying the surface of the adsorbent and the size of the cation and anion IL (Palomar et al., 2009). Hence, ionic liquids can be applied for better thermal stability, ionic conductivity, and good solubility for cellulose to give rise to ionic liquid-cellulose nanocrystals composites (IL-CNC). Moreover, Table 2 provides an insight into the several different types of adsorbents that have been modified for the practical application of lithium adsorption by surface modifications and preparation of composites. This includes activated carbon, zeolite, ion sieve, and crown ether. Nonetheless, to the best of our knowledge, date pits impregnated with cellulose nanocrystals and ionic liquid adsorbent is new and has not been investigated before.

The aim of this study, therefore, is to prepare a low-cost and environmentally friendly adsorbent by using date pits that are commonly found as an agricultural waste in Qatar as follows: (i) extraction and preparation of cellulose nanocrystals (CNCs) from locally available date pits, (2) preparation of ionic liquid/cellulose nanocrystals (IL-CNC), functionalization of date pits (DP) with the prepared IL-CNC, named as IL-CNC@DP, and application of the IL-CNC@DP and DP for the remediation of lithium ions through adsorptive batch studies from aqueous solution.

2. Methodology

2.1. Extraction of cellulose from date pits (DP) and preparation of cellulose nanocrystals (CNCs)

Date pits (DP) were obtained from a local food market in Qatar and they were washed thoroughly with distilled water to remove impurities and dirt. After drying the samples, a microphyte disintegrator was used to grind the date pits to achieve small fine particles. The particle size range used in all the experiments is 0.125–0.250 mm. Delignification of the samples by preparing 6.0% of sodium hydroxide (NaOH) in an Erlenmeyer flask with 50 g of ground date pits placed in a mechanical stirrer. The mixture was left for 4 hrs at 70 °C. This resulted in black lignin waste, which was then filtered off and the residue was undergone constant washing with distilled water to attain neutral pH. Then, the neutralized mixture was bleached by using 6.0% of sodium hypochlorite solution (NaClO). The mixture was left for 2 hrs at 70 °C. After attaining the solid residue, the product was further bleached six times and washed with distilled water to attain neutral pH to get purified cellulose.

The purified cellulose was then subjected to treatment with 64% sulfuric acid (H_2SO_4) for 1 hr under 25 °C. The acid was washed frequently by distilled water until neutral pH was achieved. Then, the CNCs were separated by centrifuging the sample at 5,000 rpm for 0.5 h. Finally, the CNCs were soaked in pure distilled water by using a dialysis membrane for 48 hrs to remove excess sulfate ions. Lastly, the dialyzed suspension of the CNCs was dispersed by ultrasonication at 600 w for 15 mins. The obtained CNCs were dried using an oven at 70 °C overnight.

2.2. Preparation of ionic liquid-nanocellulose composite (IL-CNC)

The ionic liquid (3-formyl-1-methyl pyridinium iodide, C_7H_8INO, MWt. 249.05 g/mol) was synthesized in our labs. Then, it is solubilized in DMSO (dimethyl sulphoxide) at 65 °C with constant mixing until the solution is homogenized. The already extracted CNC was then added to the mixture and left for an hour to allow time for the IL and CNC to bind and form a IL-CNC composite. A 1:1 ratio was used for IL and CNC.

Table 1
Permissible concentrations of lithium and other commonly found cations based on standards and guidelines, modified from (Ahmad et al., 2020).

Parameter	WHO (WHO, 2017)		USEPA		QATAR & GSO (GSO, 2008)	
	Drinking-Water	Irrigation Water	Drinking-Water	Irrigation Water	Drinking-Water	Irrigation Water (FAO, 1994)
Calcium (Ca^{2+}), mg/L	300***	–	–	–	80**	400
Magnesium (Mg^{2+}), mg/L	–	–	–	–	30**	60
Sodium (Na^{+}), mg/L	200***	–	60	–	80**	920
Potassium (K^{+}), mg/L	–	–	–	–	4**	2
Lithium, mg/L	–	–	–	2.5	0.05	–
Selenium, mg/L	0.04	–	0.05	0.02	0.04	–
Uranium, mg/L	0.03	–	0.02	–	0.03	–
Chromium, mg/L	0.05	–	0.1	1 (long term use) 0.1 (short term use)	0.05	0.01 (for crop) 0.2 (for grass)
Strontium, mg/L	–	–	4*	–	4	–
Aluminum, mg/L	0.2	5	0.2	20 (long term use) 5 (short term use)	0.2**	15

Note * Lifetime risk health advisory, ** KAHRAMAA requirements for water quality distribution system, *** Taste threshold, dl: detection limit.

Table 2
Comparison between different types of adsorbents.

Adsorbent	Li uptake capacity	Desorption and Regenerations	Morphology	Reference
Date pits impregnated with cellulose nanocrystals and ionic liquid	99 mg/g (pH 6 with initial concentration 100 mg/L)	Eluent concentration (0.5 M HCl and 1 M HCl), Average adsorbed concentration (35.27 mg/L), desorption (99.920% and 99.994%, respectively)	Irregular pores or cavities	This study
Functionalized titanate nanotubes	40.26 mg/g (pH 8 with initial concentration 30 mg/L)	After 3 cycles, the adsorption- desorption decreased.	Agglomeration of nanotubes	(Kamran and Park, 2020).
Polymeric porous microsphere adsorbents with crown ether	2.31 mg/g (pH 7 with initial concentration 80 mg/L)	9.13% loss of the maximum capacity after five cycles.	porous and consisted of nanoparticles	(Yuan et al., 2019).
Modified activated carbon with multiple MnO_2 nanocomposites ratios	88.5 mg/g (CAC Mn0.2 69.93 mg/g (CAC-Mn0.15) 65.04 mg/g (CAC-Mn0.12) 50.1 mg/g (CAC-Mn0.2) (pH 12 with initial concentration 20 mg/L)	Up to four cycles with 50.1–43.7 mg/g (CAC-Mn0.1), 65.04–60.21 mg/g (CAC-Mn0.12), 69.93–65.34 mg/g (CAC-Mn0.15), 88.53–83.64 mg/g (CAC-Mn0.2)	Creation of numerous cavities	(Kamran et al., 2019).
Natural and synthetic zeolites applying poly (acrylic acid)	0.5 mg/g synthetic Na-X zeolite with PAA (pH 9 with initial concentration 1000 mg/L) 5 mg/L natural clinoptilolite with PAA (Geothermal water, at pH 5.5 with initial concentration 10 mg/L)	–	Natural zeolite creates crystals and synthetic zeolite forms isometric crystals	(Wiśniewska et al., 2018a; Wiśniewska et al., 2018b)
$MnO_2{\cdot}0.4\ H_2O$ ion sieve	39.6 mg/g (pH 10 with initial concentration 10 mmol/L)	The adsorption capacity was 0.4 mmol/g after 55 cycles.	Aggregation of particles	(Xiao et al., 2015a; Xiao et al., 2015b)
1D $LiMn_2O_4$ nanorod	20 mg/g (pH 10 with initial concentration 10 mmol/L)	–	Mono-dispersed nanorods	(Zhang et al., 2010)
Nano-lithium ion sieve	37.4 mg/g (pH 12 with initial concentration 200 mg/L)	The adsorption capacity remained above 95% after recycling for 4 times.	Cluster form of floccules and nanosized particles.	(Tian et al., 2010)

2.3. Functionalization of date pits (DP) with the prepared IL-CNC

5 g of ground date pit powder (>100 μm) was thoroughly mixed with the s prepared IL-CNC. Until homogenization is achieved, the resultant IL-CNC@DP is dried in the oven for few hours at 60 °C. The newly prepared adsorbent was characterized using Fourier Transform Infrared Spectroscopy (FTIR), Scanning Electron Microscope (SEM), X-ray diffraction (XRD), Transmission Electron Microscope (TEM), Brunauer–Emmett–Teller (BET).

2.4. Preparation of lithium ions stock solution

A lithium stock solution of 100 ppm was prepared by adding 0.611 g of LiCl in a 1 L volumetric flask. LiCl (Lithium chloride, puriss. p.a., anhydrous, = 99.0% (AT), Mfr. No. 73036-100 G-F) was purchased from Sigma Aldrich. All the other chemicals were analytical grade and used without further purification, and distilled water was used throughout the experiments.

2.5. Batch adsorption of lithium

Different parameters were investigated under five pH values, namely 2, 4, 6, 8, and 10, ten initial lithium concentrations (5, 10, 15, 20, 25, 30, 35, 50, 70, and 100 mg/L), & three temperatures (25 °C, 35 °C and 45 °C). The adsorptive batch studies were conducted in 100 mL acidified glass bottles where 0.05 g of the adsorbent was added to 50 mL of the appropriate initial concentrations making sure the ratio of the adsorbent mass and the volume of the solution are 1:1 (g/mL). The bottle samples were capped and placed in the shaker for 24 h at 165 rpm. To study the pH of the adsorption system, the adjustment to its appropriate value was done by adding 1 M NaOH or 1 M HCl. Moreover, the effect of different lithium concentrations was prepared by dilutions with the optimum pH value, and then the samples are placed in a shaker for 24 h at 25 °C and 165 rpm. After each test, the spent adsorbents were filtered through a 0.2 μm syringe filter and were air-dried for further analysis using zeta potential, SEM, and FTIR. Duplicates and blanks were used in each experiment.

The initial and equilibrium lithium concentrations were analyzed by using inductively coupled plasma optical emission spectrometry (ICP-OES) (an IRIS Intrepid by ThermoFisher Scientific). The percentage of lithium removal according to Anantha et al. (2020) was calculated as per Eq. (1).

$$Removal \quad (\%) = [\frac{C0 - Ce}{C0}] \times 100 \tag{1}$$

Where C_0 and C_e are the initial and equilibrium lithium concentrations (mg/L), respectively.

2.6. Adsorption isotherm of lithium

The adsorption isotherms can be described through the relationship between the equilibrium concentration and the equilibrium adsorption capacity at a constant temperature in an aqueous solution. Four isotherm models were used in this study to determine the best-fit model for the adsorption process, namely Langmuir, Freundlich, Dubinin–Radushkevich, and Temkin isotherm models based on previous studies (Al-Ghouti and Da'ana, 2020; Zango et al., 2020).

2.7. Thermodynamic studies of lithium adsorption

Thermodynamic studies are very important for any adsorption process since they determine the spontaneity of the adsorption mechanism. One important measure of spontaneity is determined by Gibb's free energy change (ΔG°). The spontaneous reaction occurs if ΔG°, at a specific temperature, possesses a negative value. The changes in enthalpy (ΔH°) and the changes in entropy (ΔS°) are also two important thermodynamic measures. The three thermodynamic parameters (ΔG°, ΔH°, and ΔS°) were calculated according to Al-Ghouti & Al-Absi (2020), as per Eqs. (2) and (3).

$$\Delta G^\circ = -RT\ln K_L \tag{2}$$

Where R is the universal constant 8.314 J/mol.K, T corresponds to the temperature measured in Kelvin, and K_L represents the Langmuir isotherm constant. Temperature is used to express the standard enthalpy and entropy changes of adsorption.

$$\ln K_L = -\frac{\Delta H^\circ}{RT} + \frac{\Delta S^\circ}{R} \tag{3}$$

Where ΔH° and ΔS° are determined from the slope and intercept of the equation of the line that is evaluated from the plot of $\ln K_L$ vs. 1/T.

2.8. Lithium desorption study

This desorption study was carried out by using a total of 0.05 g of spent IL-CNC@DP & DP of initial concentrations of 50 ppm, 70 ppm, and 100 ppm. The spent adsorbents were tested under three different solutions: distilled water, 0.5 M HCl, and 1 M HCl. A total volume of 50 mL of each solution was used in 100 mL glass bottles. The mixture was then shaken with the required adsorbent for 24 h at 165 rpm. The spent adsorbents were filtered through a 0.2 μm syringe filter and the solution is analyzed by ICP-OES (an IRIS Intrepid by ThermoFisher Scientific). Duplicates and blanks were used in each experiment. The desorption percentage was calculated according to Eq. (4) according to Al-Ghouti & Al-Absi (2020).

$$Desorption \quad (\%) = [\frac{C0 - Ce}{C0}] \quad \times 100 \tag{4}$$

Where C_0 and C_e are the average adsorption and desorption concentration (mg/L), respectively.

2.9. Statistical analysis

Since the experimental design of the experiments was completely random, then a completely randomized design (CRD) and factorial tests are conducted. Analysis of variance (ANOVA) for two factors with replication by using Microsoft excel was used for the assessment of the relationship between the initial concentration and temperature of the batch experiments. Moreover, Analysis of variance (ANOVA) for a single factor was used for the desorption study test.

2.10. Application of DP and IL-CNC@DP to a real groundwater sample

The groundwater sample obtained from the north wells in Qatar after a rainy season in May 2019 was used to study the effectiveness and selectivity of the adsorbents. 50 mL of the groundwater sample were added to glass bottles containing 0.05 g of each adsorbent. They were placed on a shaker for 24 h at 165 rpm. The spent adsorbents are filtered through a 0.2 μm syringe filter and the solution is tested for the selectivity of metals towards the adsorbent by ICP-OES. Besides, another sample of the groundwater was analyzed for multi-element analysis without the addition of any adsorbents. Duplicates and blanks were used in each experiment.

2.11. Characterization of the adsorbents (IL-CNC@DP & DP)

Generally, in any adsorption system, the adsorbent's characterization provides the necessary understanding of the involved process and the mechanisms. Therefore, the characteristics of the adsorbents (IL-CNC@DP & DP) were determined before the adsorption process. Therefore, a scanning electron microscope (SEM) was used to evaluate the morphological characteristics of the adsorbent's surface using the JEOL model JSM-6390LV. Fourier transform infrared (FTIR) spectra were recorded using the RSpirit-T model. The FTIR analysis was conducted to interpret the functional groups present in the adsorbents. The FTIR measurements were performed over 4000–400 cm^{-1}. Moreover, the adsorbent samples were removed from the solute solution to further characterize using FTIR and SEM. Furthermore, the surface areas of the prepared materials were characterized using the Brunauer, Emmett, and Teller (BET) equation (Aim Sizer-AM301). The results were obtained by nitrogen adsorption measurements that are made at liquid nitrogen temperature, 77 K. Lastly, Zeta potential test was conducted to study the surface charge of both adsorbents in water liquid suspension at 25 °C using Zetasizer Nano ZS (Malvern Instruments). Five duplicates of each adsorbent were measured, and their averages were reported.

In addition to the characterization of the adsorbents, the obtained CNCs are characterized through SEM and X-ray diffraction (XRD) analysis. The chemically treated cellulose fibers are measured using a diffractometer (D/max 2200, Rigaku, Japan) equipped with Ni-filtered Cu Kα radiation (λ = 1.5406 Å) at 40 kV and 30 mA. The diffraction intensities were recorded between 5° and 60° (2θ angle range) at a scan rate of 5°/min. The crystallinity index (CrI, %) was measured using the Segal method (Aguayo et al., 2018). The equation of the crystallinity index is calculated as per Eq. (5).

$$CrI = [\frac{I200 - Iam}{I200}] \quad \times 100 \tag{5}$$

Where I_{200} is the maximum intensity of the diffraction at peak 200 (2θ = 22.6°) and I_{am} is the intensity of the diffraction at 2θ = 18°.

3. Results and discussion

3.1. Scanning electron microscopy (SEM) analysis

The SEM was used to study the surface of the DP and IL-CNC@DP that were used in the adsorption study of the lithium ions. Fig. 1 (A & B) shows the scanning electron microscopy (SEM) of the IL-CNC@DP before and after Li^+ adsorption. The utilization of SEM in this study can give an overview of the surface morphology of the IL-CNC@DP in addition to the alterations that might occur due to the adsorption of lithium ions. The adsorbent itself before the adsorption process occurs appears to have pores with different shapes and sizes. Moreover, these irregular pores or cavities are significant since they indicate that the IL-CNC@DP has a high surface area.

In Fig. 1. A, the magnification at 500x presents various cavities onto the whole adsorbent. Furthermore, a closer look at 25,000x demonstrates one cavity that appears to be deep and hollow. Nonetheless, it can be seen from Fig. 2B that the surface morphology appears to be slightly smoother with fewer pores and cavities. This means that the morphology of the IL-CNC@DP is enhanced and improved after the addition of IL and CNCs onto the DP. After the Li^+ adsorption process in Fig. 1B, it can be shown that the pores or cavities are still available even after the increase in temperature to 45 °C; however, they appear to be filled and blocked. This filling could be due to the deposition as aggregates of multi-layer heavy metals. At 25,000x, the surface morphology appears to be densely packed with irregular structures after the adsorption of Li^+ ions. For example, Aldawsari et al. (2017) illustrated the adsorption of heavy metals like Cd(II), Cu(II), Pb(II), and Zn(II) onto modified date pits by activated carbon. It showed morphological changes with deposited aggregates providing multi-layer adsorption of heavy metals onto the adsorbent's surface.

Fig. 2 (A & B) show the scanning electron microscopy (SEM) of the DP before and after Li^+ adsorption. In Fig. 2A, the DP structure presents a smoother morphology with no holes implying that the surface area is not yet modified and improved. Furthermore, the surface has agglomerates that are found as clusters on top of each other, shown at 5000x, whereas by looking closely at the larger magnification at 25000x, the clusters are less presenting an even surface morphology. After Li^+ adsorption onto the DP, the surface becomes more cracked and dented. At 2500x magnification, the surface appears to have holes that are elongated in shape suggesting how the adsorption process of Li^+ altered the physical appearance of the adsorbent, as shown in Fig. 2B. Additionally, the dark areas of the elongated dents are probably due to the increase of temperature to 45 °C. The SEM figures of DP are also found in previous studies where the surface morphology is almost similar to our results that were obtained (Fakhfakh et al., 2019; Mathew et al., 2018). Moreover, the study by Al-Ghouti and others (2019) showed how the SEM image of the roasted date pits presented more pores and holes upon modification by roasting the date pits at 130 °C for 3 h. In this case, no modification or alteration occurred on the date pits. In other words, the sample used in this study is not modified to enhance the surface area of the adsorbent to reveal more adsorption sites. Hence, these results are

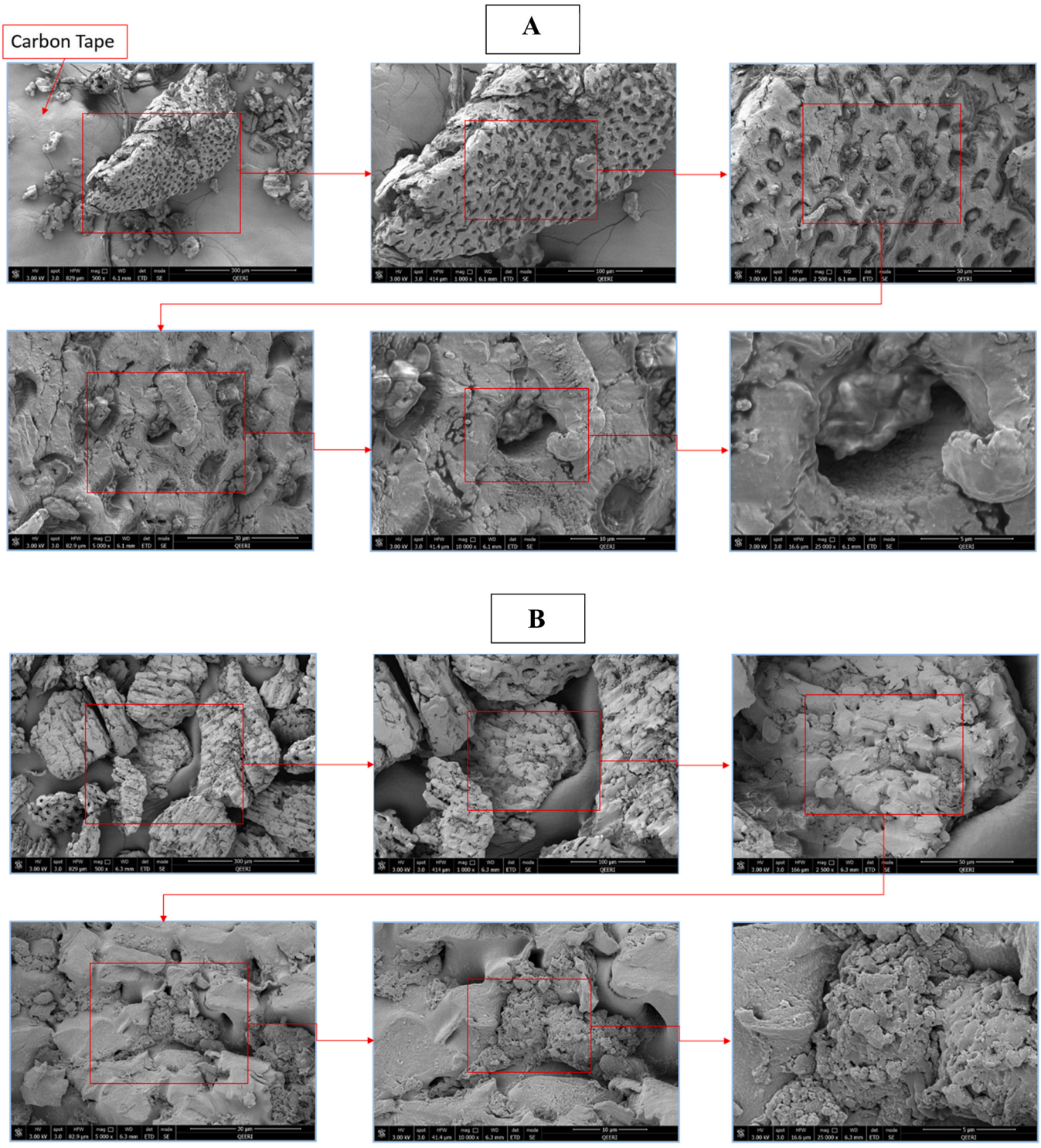

Fig. 1. SEM images of the IL-CNC@DP of 0.125–0.250 mm size before and after adsorption. (**A**) Before the treatment under 25 °C. (**B**) After Li^{+} adsorption at 100 ppm with pH 6 under 45 °C.

confirmed by the BET analysis since the specific surface area of the DP was found to be 2.126 m^2/g, where the IL-CNC@DP has a specific surface area of 4.254 m^2/g.

Furthermore, to prove the presence of CNC, SEM analysis was also performed, and the results are demonstrated in Fig. 3. It is clearly shown that the acid hydrolysis treatment by sulfuric acid has converted the large porous pieces of cellulose into smaller pieces and fragments with a crystal-like morphology. The resulted CNC possesses a porous network with a lamellar structure. Furthermore, at high magnification, the SEM images display cellulose microfibrils with structures that are highly packed due to the strong hydrogen bonding of the intermolecular and intramolecular forces. In addition, the crowded structure of the microfibrils is also due to the presence of van der Walls forces (Trache et al., 2016).

3.2. Fourier transform infrared (FTIR) analysis

It is clearly evident that the modification performed by IL and CNCs

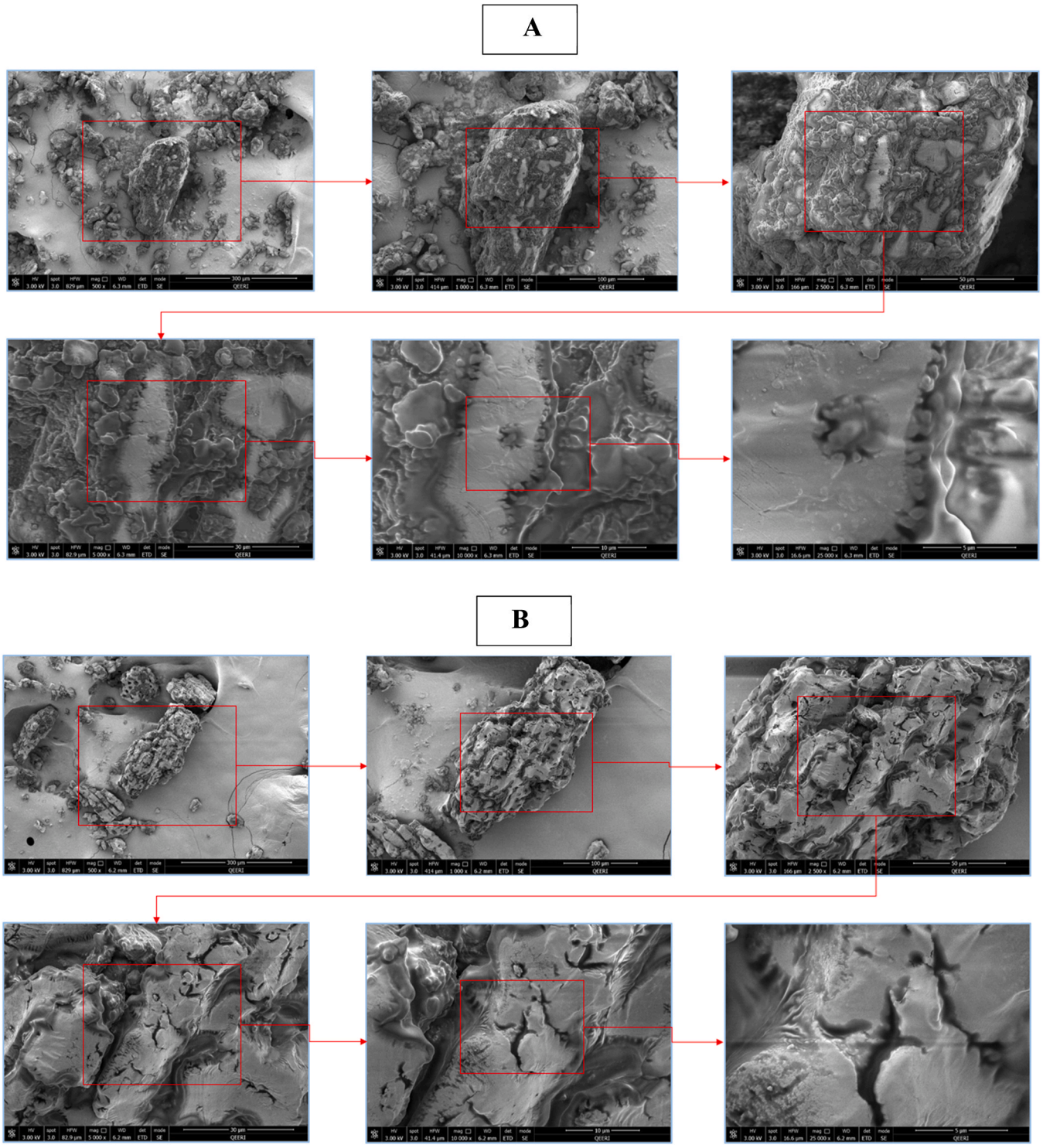

Fig. 2. SEM images of the DP of 0.125–0.250 mm size before and after adsorption. (**A**) Before the treatment under 25 °C. (**B**) After Li^+ adsorption at 100 ppm with pH 6 under 45 °C.

did occur, as shown in Fig. 4. It shows that the adsorbent IL-CNC@DP has less intense peaks in comparison to the DP due to the modification performed. One important finding that the FTIR spectra presented is the bending of the peaks in the 3000 cm^{-1} - 3500 cm^{-1} regions of IL-CNC@DP. The peaks at 3348 cm^{-1} and 3455 cm^{-1} are attributed to the N – H stretching vibration absorption peak found in the adsorbent (Zheng et al., 2019). This means that there is a hydrogen bonding between the nitrogen of the IL and the hydroxyl groups of the CNCs. Moreover, that indicates why the broad O-H stretching band at 3311 cm^{-1} in the DP is found and in the IL-CNC@DP adsorbent, the peak is starting to shift to present bending peaks (Abu-Thabit et al., 2020). The bands at 2854 cm^{-1} and 2921 cm^{-1} that are represented by the C-H stretching vibrations of the methoxyl groups that are related to the lignin component are found in the IL-CNC@DP adsorbent (Abu-Thabit et al., 2020). Nonetheless, it can be inferred that the intensity and sharpness of the absorption bands decreased in comparison to the DP and this can be explained by the fact that the CNC sample that was used to prepare the IL-CNC@DP had less lignin content that was removed by

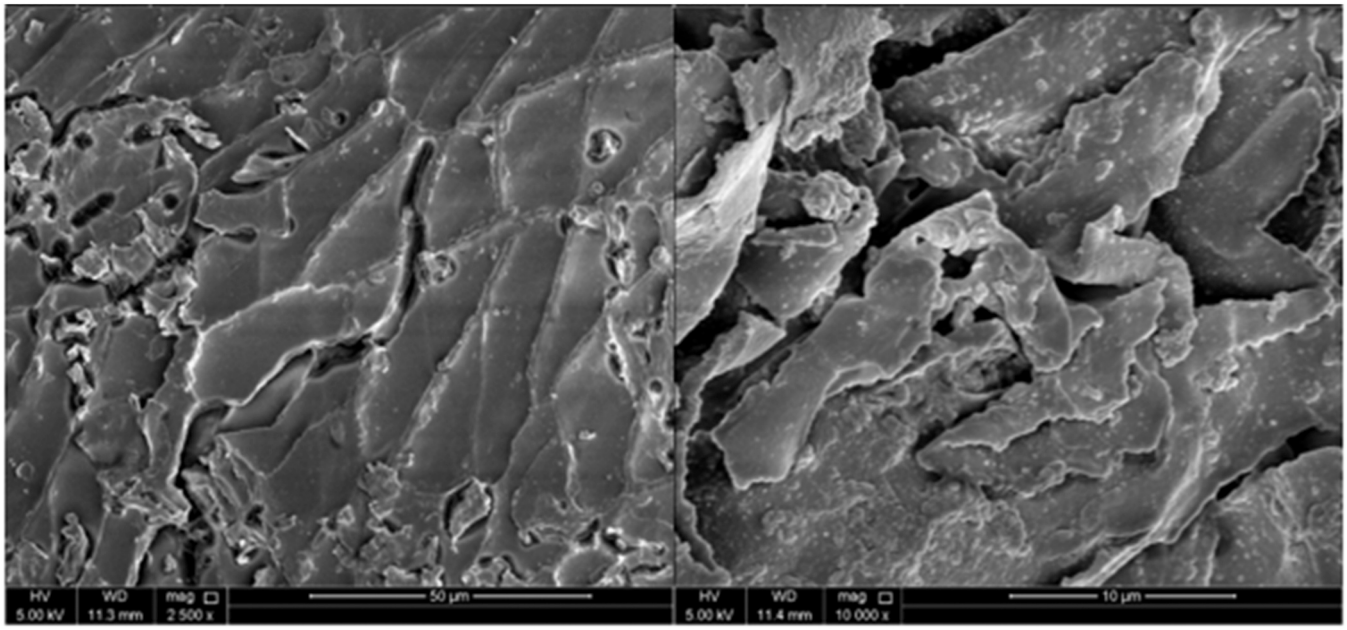

Fig. 3. Schematic illustration of SEM results of the surface morphology of CNC.

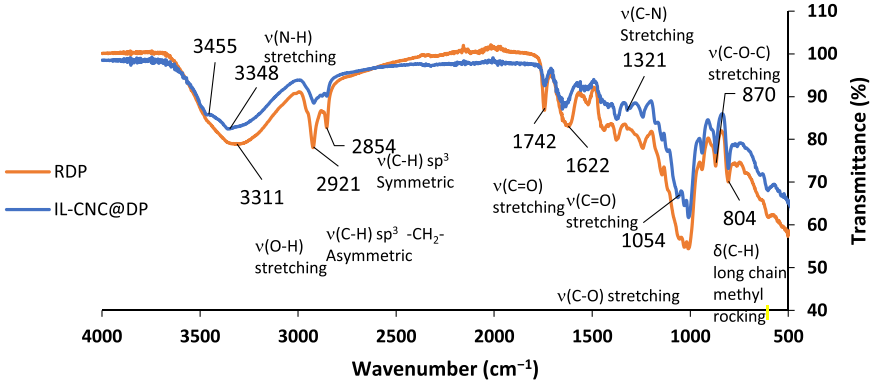

Fig. 4. FTIR spectrum of the unmodified DP and the modified IL-CNC@DP adsorbents.

the hydrolysis treatment to obtain pure CNC.

To understand the modification better, the peak at 1742 cm^{-1} corresponds to the hemicellulose of the DP. Nevertheless, this peak was found in the IL-CNC@DP adsorbent; indicating the presence of aldehyde corresponding to the C═O stretching of the IL, demonstrated in Fig. 4 (Gholami-Bonabi et al., 2020). Furthermore, there are other absorption peaks that represent the lignin components in the range of 700 cm^{-1} - 900 cm^{-1}, which are related to the C-H functional group of the aromatic hydrogen compound (Morán et al., 2008). The peaks are visible in both adsorbents because date pits were used as the supporting mechanism in the case of the modified adsorbent. In addition, the peak at 1622 cm^{-1} correlates to the C═O asymmetric stretching band of the carboxyl group of glucuronic acid in hemicellulose and also to the conjugated carbonyl of lignin stretching (Zhuang et al., 2020). It can be seen that in the IL-CNC@DP adsorbent the peak shifted slightly to the left and became narrower due to the modification performed on the sample that removed part of the hemicellulose and lignin components. A closer look at the FTIR spectra demonstrates a peak that is only visible in the novel adsorbent at 1321 cm^{-1} that represents the C-N stretching of the IL that was used to modify the DP. Lastly, the peak at 1054 cm^{-1} in the IL-CNC@DP corresponds to the C–O stretch in cellulose and hemicellulose (Al-Ghouti et al., 2010). From Fig. 4, it can be shown that this peak is more evident in the IL-CNC@DP sample more than the DP possibly due to more cellulosic components from the CNC.

Fig. 5 A demonstrates the FTIR spectra of the unloaded IL-CNC@DP and Li^+ loaded IL-CNC@DP at an initial concentration of 100 mg/L. Visible differences can be detected in the FTIR spectra regarding the absorbance shapes and locations of the bands but the absorbance pattern did not significantly change after the adsorption of Li^+. For example, the bending of the peaks in the 3000 cm^{-1}–3500 cm^{-1} region and 3348 cm^{-1} and 3455 cm^{-1} that corresponds to the N—H stretching vibration absorption became more intense and sharper after the adsorption of the Li^+ ions. The adsorption of Li^+ onto IL-CNC@DP caused a dip in the two peaks as they become narrower comparing to the unloaded adsorbent. Additionally, the O-H band at 3311 cm^{-1} in the unloaded IL-CNC@DP is broad as it started to present bending peaks but after the adsorption of Li^+, the width of the entire band became narrower. As for the C-H stretching vibrations of the methoxyl groups at 2851 cm^{-1} and 2920 cm^{-1} after adsorption, the band's intensity and sharpness are signifying that the lignin functional group that is found from the date pits is expected to contribute to the Li^+ binding. Moreover, the peak at 804 cm^{-1} that also represents the lignin components related to the C-H functional group demonstrates more intensity and sharpness after the adsorption of Li^+ takes place. As for the unconjugated C═O hemicellulose functional group at 1742 cm^{-1}, the peaks remained the same before and after adsorption suggesting that perhaps this functional

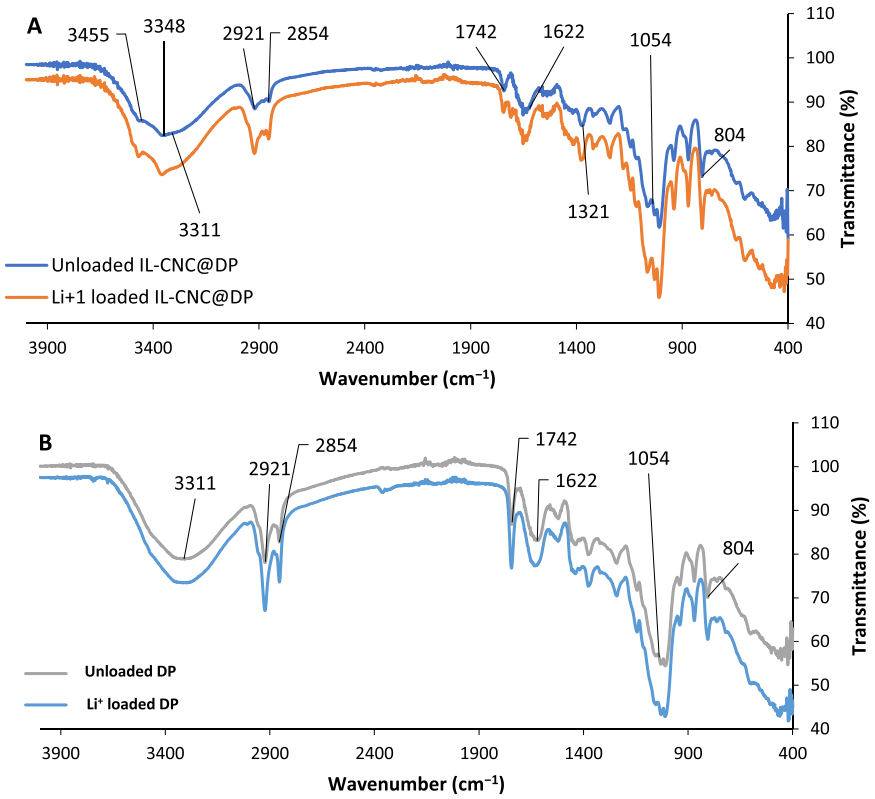

Fig. 5. FTIR spectra of the IL-CNC@DP and DP before and after Li^+ ions adsorption. (A) IL-CNC@DP and (B) RDP. Experimental conditions for Li^+: particle size: 0.125 mm−0.250 mm, adsorbent mass: 0.05 g, temperature: 45 °C, concentration: 100 mg/L, solution volume: 50 mL, pH: 4 & 6, and contact time: 24 h.

group did not contribute to the adsorption process for Li^+ adsorption. Although looking closely at the FTIR spectra of Li^+ loaded IL-CNC@DP, it can be shown that a small peak can be detected at around 1707 cm^{-1}. This means that the hemicellulose functional group from the date pits did contribute to the Li^+ binding for the adsorption process. Furthermore, the peak 1622 cm^{-1} corresponding to C═O stretching of hemicellulose and lignin did not change for the Li^+ loaded IL-CNC@DP. The peaks that were observed at 1321 cm^{-1} and 1054 cm^{-1} demonstrated no alterations in the absorbance bands after the adsorption of Li^+.

Fig. 5B shows the FTIR spectra of the unloaded DP and Li^+ loaded DP at an initial concentration of 100 mg/L. For the unloaded DP, a strong inter- and intra-hydrogen bonding (O-H) stretching absorption is seen at 3311 cm^{-1} that occurs in cellulose components. Furthermore, the peaks at 2854 cm^{-1} and 2921 cm^{-1} that correspond to the lignin content show a sharp dip after the loading of Li^+ ions. This proposes that the lignin functional group found in DP after the adsorption of Li^+ ions contributes to the adsorption process. Furthermore, there are other absorption peaks that represent the lignin components in the range of 700 cm^{-1} - 900 cm^{-1}, such as band 804 cm^{-1}, where no differences in adsorption of Li^+. As for the unconjugated C═O hemicellulose functional group at 1742 cm^{-1}, the peak became sharper after the adsorption of Li^+ ions. This can suggest that the hemicellulose functional group found in DP plays a role in the adsorption process. Also, the peak at 1622 cm^{-1} and 1054 cm^{-1} did not change for the Li^+ loaded IL-CNC@DP demonstrating no significant changes in the absorbance peaks. Similarly, Xu et al. (2020), found a strong peak at 1731 cm^{-1} corresponding to the C═O group on the used cellulose-based adsorbent for the removal of lithium. These results agreed well with the XPS analysis in which showed that there are peaks of O_1 (oxygen) and C_1 (carbon) with a binding energy of 55.6 eV that occurred after adsorption (Xu et al., 2020).

3.3. X-ray powder diffraction (XRD) analysis

The XRD analysis of the extracted cellulose that is successfully converted to nanocellulose is indicated by the crystalline nature of the fibers, as shown in Fig. 6. The XRD spectrum of CNC is represented by diffraction peaks at 2θvalues 15.8°, 22.5°, and 33.5°. These peaks correspond to the lattice planes (Miller index) 110, 200, and 004, respectively (Guo et al., 2020; Zheng et al., 2019; Chandra et al., 2016). The peaks indicate that the typical cellulosic structure was maintained and preserved. It also shows that the chemical treatments done to obtain CNCs by using sulfuric acid did not change the integrity of the original cellulose crystal (Marett et al., 2017). The sharp diffraction peak at $2\theta = 22.6°$ proves that high crystallinity is present as reported by Trilokesh and Uppuluri (2019). In the current study, this sharp peak is present at 22.5°, which proves the high crystallinity of cellulose extracted from RDPs is present. The order of the crystalline arrangements in the CNC sample is reported due to the formation of inter and intramolecular H-bonding by the hydroxyl groups. This H-bonding tends to limit the movement of the cellulosic chains that causes the chains to align next to one another, which forms the crystallinity of the cellulose (Chandra et al., 2016). From Eq. (5), the crystallinity index is calculated for the CNC sample. It was found that the apparent crystallinity of CNC is 69.99%, which demonstrates high crystallinity that is attributed to the effective removal of the non-crystalline regions due to the consecutive chemical treatments performed on RDPs.

3.4. Zeta potential analysis

The zeta potential analysis was performed to study the stability of the adsorbents (IL-CNC@DP & RDP) in a solution and to determine the charges that are available in the interface between the adsorbents and the solution. This type of analysis is particularly important since it demonstrates the effect the adsorption has on the electrostatic

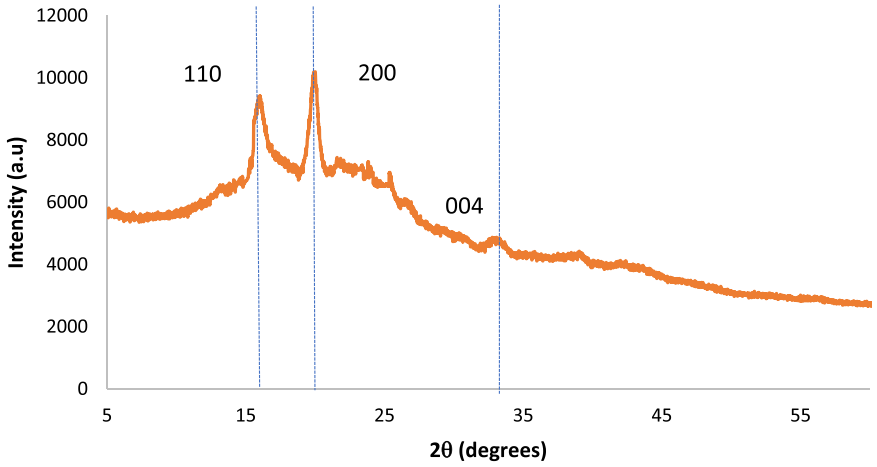

Fig. 6. XRD pattern of the CNC.

attractions and repulsion forces, which tend to impact the adsorptive capacities of the adsorbents towards lithium ions (Engwayu and Pawlik, 2020). As a result, the zeta potential was determined for modified IL-CNC@DP & unmodified RDP adsorbents in water with pH ≈ 6, which represents the optimum pH value of both adsorbents due to their high adsorption capacities. The zeta potential was found to be equal to − 28.85 and − 27.76 for IL-CNC@DP and RDP, respectively. Since the values of the obtained zeta potential fall in the range of − 20 to − 30 mV, it clearly indicates the moderate stability of the synthesized adsorbent (Singh et al., 2018). The negative values show that the charges in the interface between the adsorbent and solution that contains lithium ions are negative, thus establishing electrostatic attraction forces that support the adsorption process. However, the zeta potential values for IL-CNC@DP are slightly more negative than the zeta potential values for RDP. This means that IL-CNC@DP is more stable in the adsorption solution than RDP and more electrostatically negative, which presents more electrostatic attraction forces towards the positively charged lithium ions. This is also supported by the fact that IL-CNC@DP achieved higher adsorption efficiencies than RDP. Similarly, Nizam et al. (2021) investigated the zeta potential value of activated carbon derived from date palm seeds and found that zeta potential value equals − 27 mV. However, Khalil et al. (2021) developed a date palm extract coated with PEG nanoemulsion and found that the negativity of the analyzed zeta potential declined compared with the naked date palm extract as it was − 24.6 and after surface coating with PEG it was found to be 3.23. Furthermore, Irfan et al. (2020) synthesized IL-mediated silver nanoparticles using extract of oil palm kernel (OPK) and investigated its zeta potential value over 30 days and results showed that it was in the range of − 18.7 mV and − 21.4 mV.

3.5. *Effect of pH on lithium adsorption*

The effect of pH on the percentage removal of lithium ions from the aqueous solution by IL-CNC@DP & DP is illustrated in Fig. 7. Studying the effect of pH on the adsorption of Li^+ onto IL-CNC@DP can give an idea about the adsorption mechanisms and the efficiency removal so it can be applied on a larger scale to treat groundwater in Qatar.

It is important to note that pH is one of the significant parameters impacting metal ions' adsorption (Liang et al., 2020; Xu et al., 2020; Xiao et al., 2015a, 2015b). Lithium, an alkaline-earth metal, is found in a solution as a protonated form with an atomic number of three (Ahmad et al., 2020). This means that at a lower pH value, H^+ ions at high concentrations can compete with the metal ions for the active sites to form protonation. Hence, the percentage of Li^+ removal tends to decrease. The increase in the pH value demonstrated an increase in the removal capacity of Li^+ by both adsorbents, IL-CNC@DP and DP. In more detail, the Li^+ adsorption onto the IL-CNC@DP displays a trend, where it shows as the pH value increases from 2 to 10, the adsorption also increases. The lowest adsorption was observed at pH 2, which was found to be at 55%. On the other hand, the highest percentage of removal was found to be at pH 6 and 8 at 90%. The differences between the adsorption behaviors are due to the fact that the solution at low pH possesses highly protonated H^+ ions where it competes with the protonated Li^+ for the active sites on the negatively modified adsorbent. As

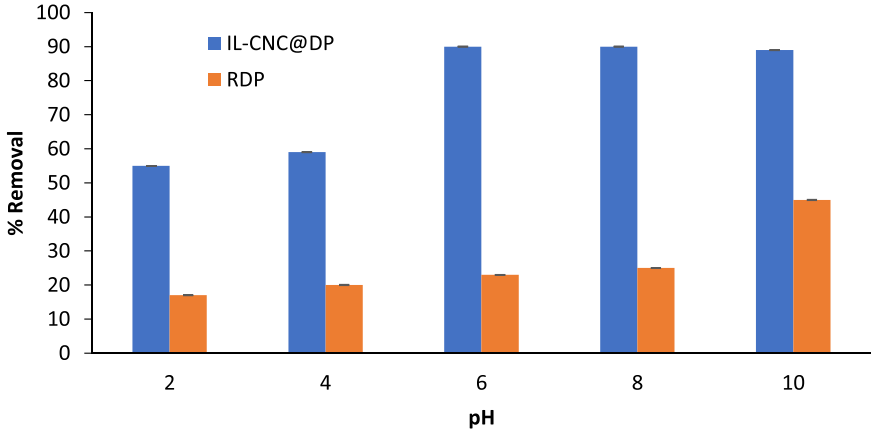

Fig. 7. Percentage removal of Li^+ from solution by IL-CNC@DP and DP at different pH values. Experimental conditions: particle size: 0.125–0.250 mm, adsorbent mass: 0.05 g, temperature: 25 °C, initial Li^+ concentration: 100 ppm, solution volume: 50 mL, and contact time: 24 h.

a result, this causes lower adsorption for low pH values. Furthermore, at low pH values, the H^+ ions might desorb the previously bound metals back into the solution (Hawari et al., 2014). It is worth noting that at low pH, protonation of the surface functional group occurs; hence, a positive charge would be formed on the surface. On the other hand, while at high pH, the surface loses its protons and it will become anionic (Heibati et al., 2014). Moreover, at pH 4, the percentage removal slightly increased as the competing behavior in the solution decreased, which allowed the adsorption to be enhanced. At pH 6, there is a significant increase in the removal efficiency where it increased to 90%. This also could be explained by the fact that electrostatic attraction forces and hydrogen bonding existed between the protonated Li^+ and the less protonated IL-CNC@DP adsorbent surface, which enhanced the percentage of Li^+ removal. Zhong et al. (2021) investigated the adsorption mechanism of lithium into lithium/aluminum layered double hydroxides and XPS results showed that electrostatic interaction and hydrogen bonds are responsible for the adsorption process. Nevertheless, as the pH becomes more basic at values 8 & 10, it will be concentrated with more OH^- ions, therefore the attraction forces increased between the positively charged Li^+ and the negatively charged surface of the adsorbent. This will allow more adsorption of Li^+ to occur and enhance the removal percentage at high pH values. Another explanation could be due to "faked" adsorption behavior due to the presence of Li^+, and at high concentrations of OH^- ions, lithium hydroxides (LiOH) in the solution forms. Precipitation of metals forms metal hydroxides at high pH values is explained in recent studies (Eggermont et al., 2020). Therefore, the high adsorption behavior could be due to the behavior of metals and not the adsorption mechanism itself. Another study by Al-Ghouti et al. (2010) demonstrated the adsorption mechanisms of two metals onto DP under different pH values. The results show a similar trend in the fact that the adsorbent under basic conditions and less protonated forms, the precipitation of metals occurs. To try to understand the modification better, the DP was used as a control to compare with the novel adsorbent; IL-CNC@DP. The control adsorbent shows a similar trend as the one observed by the modified adsorbent. In other words, at pH 2 the percentage of solute removal was found at 17%, and at pH 10, the percentage of solute removal increased to 45%. The pH values at 4, 6, and 8 have minor differences regarding their adsorption efficiency, where the values are 20%, 23%, and 25%, respectively.

This also proves that the utilization of DP alone without modifications is not as efficient enough to be used as adsorbents for the selective adsorption of lithium in comparison to the modified adsorbent, IL-CNC@DP. Besides, it further proves that the modification on DP by using CNCs and IL occurred as it improved its adsorption capabilities by enhancing its functional groups. Furthermore, other studies support the fact that cellulose is an important polymer for the adsorption of Li^+ elements at high pH values. For example, CNCs were used as bio-templates to synthesize mesoporous films as a way to enhance the surface area and physicochemical properties for the adsorption of Li^+. The mesoporous film template by CNCs demonstrates an increase in the Li^+ adsorption capacity with increasing pH from 3 to 7. Moreover, they stated that the acidic nature of the adsorption sites is influenced by the decrease in pH as a result of the ion exchange system and the lower extent of dissociation of functional groups of the mesoporous film (Zheng et al., 2019). Another study by Xu et al. (2020) confirmed that the Li^+ uptake decreased at low pH values due to the competition of H^+ and Li^+ ions against each other on the active sites of the cellulose microsphere adsorbent.

Therefore, according to the obtained results for Li^+ removal, the optimum pH value was found to be at 6 and 8, but as previously mentioned, at high basic conditions, lithium hydroxides (LiOH) in the solution will tend to form. Thus, it will not be practical to proceed with the following experiments at such pH value, therefore a more moderate pH value was selected which is 6. The differences between pH 6, 8, and 10 removal efficiencies are not that significant between one another. Lastly, this pH value is more economically feasible and sustainable for the environment since it does not require huge amounts of NaOH or HCl when modifying the pH values. The continuation of the DP control experiment was also conducted at pH 6 for the same reasons mentioned.

3.6. Effect of initial concentration on lithium adsorption

Understanding the effect of metal concentrations on the adsorption capacities of adsorbents is also essential for Li^+ recovery. Keeping in mind that the concentration of the targeted Li^+ impacts the efficiency, capacity, and adsorption mechanisms in a solution. Moreover, it is important to mention that breaking down the adsorbent into smaller particles tends to open the sealed channels on the adsorbent; hence, the adsorption rate will tend to increase. Therefore, in this study smaller particle sizes of the adsorbent that ranged from 0.125 mm to 0.250 mm were used. Furthermore, most studies correlated the practicality of using cellulose nanofibrils (CNF) as adsorbents for metal ions, and only a few studies reported on CNCs (Mahfoudhi and Boufi, 2017).

Fig. 8 illustrates the adsorption capacity for Li^+ onto IL-CNC@DP and DP at multiple concentrations. The metal concentrations that were used with an optimum pH value of 6 for both adsorbents present a general trend in results. The steady constant increase of adsorption capacity with the increasing Li^+ concentrations is evident for both adsorbents. It is apparent that the adsorption capacity of IL-CNC@DP is the highest in comparison to DP. This is also confirmed by the previous results that present the adsorption efficiency of Li^+ at several pH values was the highest for IL-CNC@DP in contrast to DP. It is important to mention that nanocellulose composites are significant adsorbents that can be used to adsorb many classes of pollutants including metals (Tao et al., 2020; Mahfoudhi and Boufi, 2017). Therefore, the modification made onto the DP, where IL was used as a linkage between the surface of the DP and the CNC promoted better and enhanced removal percentages. It can be clear that the adsorption capacity of Li^+ onto IL-CNC@DP presented a steady increase overall in the concentrations used. Nonetheless, the adsorption capacity onto DP was much less under the same concentrations used. According to Hilal et al. (2012), the removal efficiency increased as the concentration increased for Cu^{2+} and Cd^{2+} metal ions. This is due to the overall mass transfer driving force. Therefore, in this study, the constant increase in the adsorption capacity along with the increase in concentration is directly linked to the increase in metal mass transfer onto the adsorbent's surface of the CNC. The IL-CNC@DP proved that adsorption was highest at high initial concentrations due to the increase in Li^+ mass transfer and collision between the ions and the active binding sites (Manirethan et al., 2019). Furthermore, the enhancement of the adsorption capacity of the modified adsorbent with an increase in the initial concentration of Li^+ ions is due to the increased diffusion of Li^+ (Samra et al., 2014). In other words, the internal diffusion of the ions to the pores of the adsorbent is one of the driving forces that enhance the adsorption capacities (Girish and Murty, 2016). To sum up, the IL-CNC@DP had a better mass transfer, collision, and diffusion, which resulted in enhanced adsorption capacity in comparison to DP.

To be more specific, the adsorption capacity (qe) delivers information about the amount of Li^+ adsorbed per gram of adsorbate at equilibrium (mg/g). Therefore, the adsorption capacities for the adsorption of Li^+ onto IL-CNC@DP were found to be 4.47, 9.40, 14.34, 19.29, 24.25, 29.22, 34.21, 49.19, 69.18, and 99.17 mg/g for Li^+ concentrations of 5, 10, 15, 20, 25, 30, 35, 50, 70, and 100 mg/L, respectively. On the other hand, the adsorption capacities for the adsorption of Li^+ onto DP were found to be 0.59, 1.64, 2.57, 4.65, 6.26, 9.60, 13.73, 20.93, 31.38, and 53.02 mg/g for Li^+ concentrations of 5, 10, 15, 20, 25, 30, 35, 50, 70, and 100 mg/L, respectively. The high adsorptive capacity of IL-CNC@DP towards Li^+ was more prominent at high Li^+ initial concentrations due to the fact that more binding sites were available at high metal concentrations that promoted better filling inside the pores of the adsorbent surface. Furthermore, studies by Al-Ghouti et al., (2017, 2019) demonstrated that the adsorption increased with the increase in

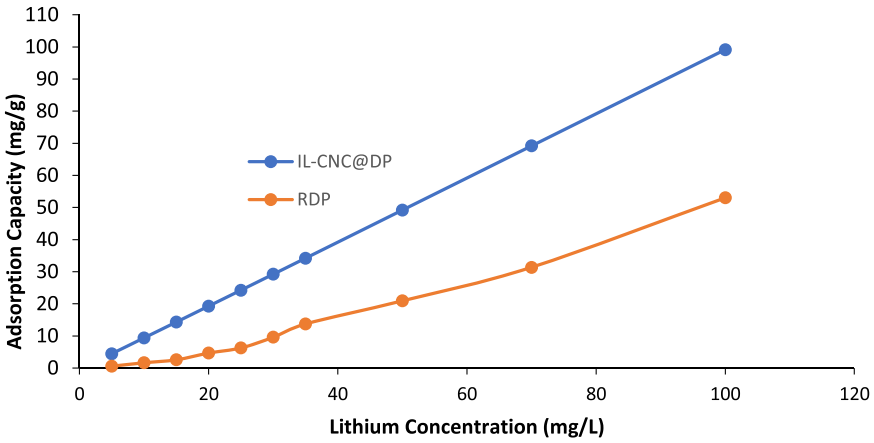

Fig. 8. Effect of initial concentration on the IL-CNC@DP & DP at different concentrations on Li^+ adsorption. Experimental conditions: particle size: 0.125 mm – 0.250 mm, adsorbent mass: 0.05 g, temperature: 25 °C, initial Li^+ concentrations: 5, 10, 15, 20, 25, 30, 35, 50, 70, and 100 mg/L, solution volume: 50 mL, pH: 6, and contact time: 24 h.

concentration because of collision and enhance mass transfer forces between the Li^+ and the adsorbent itself. Also relying on the adsorption capacity concept, the adsorption mechanisms through adsorption isotherm models will be presented later on.

In this study, concentrations above 100 mg/L for IL-CNC@DP were not employed since the adsorption capacity of Li^+ reached 99 mg/g with 99% adsorption efficiency at 100 mg/L of initial metal concentration. It reached equilibrium due to the increase in Li^+ concentrations that facilitated the mass transfer driving force that increased the adsorption onto the CNC available surface-active sites. Nevertheless, it is expected that the adsorbent eventually will have limited available active sites; therefore, the adsorption capacity will reach a plateau (Jiang et al., 2020). It is also important to mention that the higher adsorption capacity of IL-CNC@DP in comparison to DP could be attributed to the

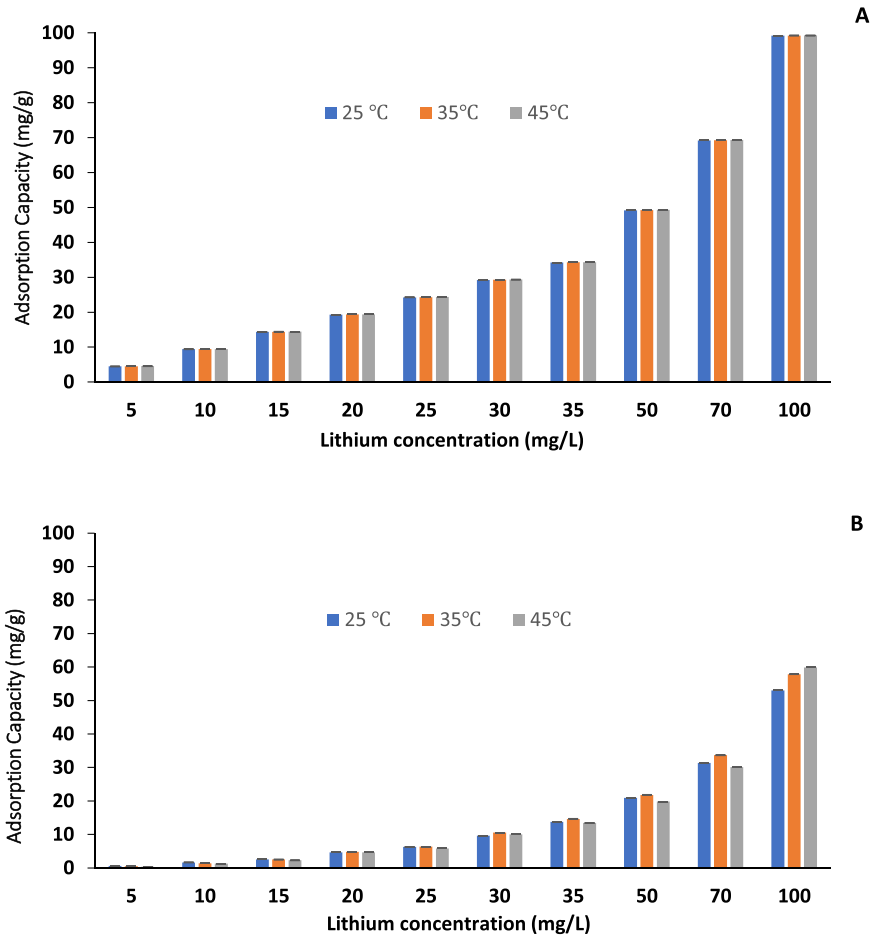

Fig. 9. Effect of temperature on the IL-CNC@DP (A) and DP (B) at different concentrations on Li^+ adsorption. Experimental conditions: particle size: 0.125 mm – 0.250 mm, adsorbent mass: 0.05 g, temperature: 25 °C, 35 °C, & 45 °C, initial Li^+ concentrations: 5, 10, 15, 20, 25, 30, 35, 50, 70, and 100 mg/L, solution volume: 50 mL, pH: 6, and contact time: 24 h.

adsorbents' characteristics. This means that the characterization of the adsorbent can enhance the selectivity of any pollutant. In this study, the BET results that were obtained demonstrated that the DP adsorbent had a specific surface area of 2.126 m^2/g with a pore volume of 0.008611 cm^3/g. After modification, the specific surface area of the IL-CNC@DP adsorbent was found to be 4.254 m^2/g with a pore volume of 0.015527 cm^3/g. Therefore, such characterization proves why Li^+ favors adsorption onto the surface of IL-CNC@DP more than DP since it has higher pore volume and surface, which provides more active binding sites; therefore, more adsorption towards Li^+. This is also supported by the SEM results, where the surface of IL-CNC@DP contains more pores and dents in comparison to the smoother surface of DP. The adsorption of Li^+ can reach its all-time high at 99 mg/g at 100 mg/L by using the IL-CNC@DP.

3.7. Effect of temperature on lithium adsorption and its thermodynamics

Another important parameter that plays an important role in any adsorption process is temperature. Any batch adsorption process depends greatly on the surrounding temperature for the removal and recovery of metals. The effects of temperatures on Li^+ adsorption onto IL-CNC@DP and DP were investigated at different temperatures and the results are shown in Fig. 9 (A & B). Fig. 9A shows a linear increase of Li^+ adsorption onto IL-CNC@DP with increasing initial concentrations as it directs the accessibility of several active sites as the Li^+ concentration increases. It is evident that when the adsorption process was conducted at 25 °C, 35 °C, and 45 °C, the amount of Li^+ being adsorbed did not fluctuate much and that the effect of temperature did not contribute as a major factor in this study. However, there is an increase in the adsorption capacity and efficiency as the temperature increases, but the differences between the temperatures are insignificant. These findings are noteworthy since the increase in temperature requires more energy and cost, therefore room temperature experiments are more practical and affordable. Moreover, this means that the IL-CNC@DP is effective enough to be physically active at low temperatures rather than utilizing high temperatures. Despite that, recent findings validate that the effect of the temperature factor does in fact contribute to the adsorption capacity (Al-Ghouti & Al-Absi, 2020; Al-Ghouti and Da'ana, 2020; Al-Ghouti et al., 2019). In this study, the temperature factor did not play a significant role in the IL-CNC@DP. Regardless, analysis of variance (ANOVA) was used to assess the significance of the results in this study. A two-factor ANOVA test was conducted to study the relationship between the initial Li^+ concentration and temperature. The two-factor ANOVA results of Li^+ onto IL-CNC@DP show a significant difference at a p-value of 0.03, but experimentally the results are not significant.

Therefore the results show that the adsorption capacity of Li^+ at 5 mg/L onto IL-CNC@DP is found to slightly increase from 4.47 mg/g (89.46%) at 25 °C to 4.50 mg/g (90.06%) at 35 °C to 4.54 mg/g (90.96%) at 45 °C. Comparing these results to the adsorption capacity of Li^+ at 100 mg/L, it was found that it also increases slightly from 99.1 mg/g (99.17%) at 25 °C to 99.2 mg/g (99.23%) at 35 °C to 99.2 mg/g (99.25%) at 45 °C; indicating the availability of active sites on the surface of the adsorbent at increasing initial concentrations. Therefore, water treatment processes that are concentrated with Li^+ can be recovered at low temperatures using IL-CNC@DP at high initial concentrations for optimum and maximum recovery of Li^+. While on the other hand, Fig. 9B shows a linear increase of Li^+ adsorption onto DP with increasing initial concentrations, but fluctuations are demonstrated under the three different temperatures. The adsorption capacity of Li^+ at 5 mg/L onto DP is found to decrease from 0.58 mg/g (11.71%) at 25 °C to 0.51 mg/g (10.32%) at 35 °C to 0.32 mg/g (6.57%) at 45 °C. This trend of decreasing with increasing temperatures is shown up until initial concentrations of 15 mg/L and then the trend started to show other variations. One constant result was observed for DP was that at initial concentrations of 20 until 70 mg/L, the optimum adsorption capacity was found at 35 °C. Later, it showed a constant trend of increasing that indicates the incapability of the molecules to naturally adhere on the surface of the DP adsorbent due to the presence of few available active sites. Similar results are shown by a recent study by Al-Ghouti et al. (2019), where the adsorption of mercury at 25 °C increased with increasing concentrations, but at 35 °C and 45 °C, the adsorption started to show fluctuating trends of increasing and decreasing. In this study, at 100 mg/L, the optimum temperature was found to be 45 °C, although at 35 °C the adsorption capacity is still high. Overall, it can be concluded that moderate temperature is more favored by the adsorption process onto DP. Besides, analysis of variance (ANOVA) was used to assess the significance of the results in this study. A two-factor ANOVA test was conducted to study the relationship between the initial Li^+ concentration and temperature. The two-factor ANOVA results of Li^+ onto DP show a significant difference at a p-value of 3×10^{-8}.

Based on the obtained results, the thermodynamics calculations for Gibbs free energy, enthalpy, and entropy were analyzed for both adsorbents at 25 °C, 35 °C, and 45 °C. This was performed to understand the behavior of the reactions that took place under different temperatures. From Table 3, the values of ΔG° are found to have a negative value throughout all the experiments, indicating that the adsorption of Li^+ onto IL-CNC@DP and DP are feasible, spontaneous, and do not need an external driver for the reaction to take place. Similarly, the negative value of ΔH° for all the experiments indicates that the reactions were exothermic. Lastly, the negative value of ΔS° confirmed that the adsorption of Li^+ on the surface of the adsorbents is an associated mechanism (Al-Ghouti et al., 2019; Imran Din et al., 2013).

The calculation of the thermodynamics at 25 °C, 35 °C, and 45 °C was carried out based on the previously mentioned Eqs. (2) and (3), where the Li^+ concentrations varied. The ΔG° values for the modified adsorbent IL-CNC@DP were − 11.21 kJ/mol, − 9.08.11 kJ/mol, and - 6.96 kJ/mol at 25 °C, 35 °C, and 45 °C, respectively. According to the negative values obtained for Gibbs free energy, it can be concluded that the adsorption of Li^+ onto IL-CNC@DP was spontaneous at all the studied temperatures. While the values of ΔH° and ΔS° were − 74.57 kJ/mol and − 0.21 kJ/mol, respectively. The ΔH° verifies the previous results of the effect of temperature on the adsorption of Li^+ onto IL-CNC@DP, where utilization of different temperatures did not have an effect on the adsorption process. As for ΔS° results, it does not favor the high level of disorder in the adsorption process. For the DP, the ΔG° values were − 12.25 kJ/mol, − 11.11 kJ/mol, and − 9.98 kJ/mol at 25 °C, 35 °C, and 45 °C, respectively. The values of ΔH° and ΔS° were − 46.05 kJ/mol and − 0.11 kJ/mol, respectively.

3.8. Adsorption isotherms of lithium

The linear adsorption isotherms for Li^+ adsorption onto IL-CNC@DP and DP at 25 °C, 35 °C, and 45 °C were investigated in order to define the relationship of the amount of Li^+ adsorbed per gram of adsorbate at equilibrium (q_e) and equilibrium concentration of adsorbate (C_e) at constant temperature and pH. Therefore, four isotherm models were tested using Langmuir, Freundlich, Dubinin–Radushkevich, and Temkin models, and their parameters and constants are shown in Table 4 for IL-CNC@DP and DP. Based on general observation, the isotherm models for the IL-CNC@DP and DP show high values of R^2. This means that the adsorption of Li^+ adsorption onto the IL-CNC@DP and DP could follow any of the mentioned models (Magdy et al., 2018). Both, the IL-CNC@DP and DP obtained the highest R^2 value with the Freundlich isotherm model.

It can be seen that the values of R^2 of the Langmuir model of the IL-CNC@DP and DP follow the model's theory, although the R^2 value of the IL-CNC@DP is slightly better than the DP. In general, this means that Li^+ molecules form a homogenous monolayer on the surface of both adsorbents along with different adsorption mechanisms with no interactions of molecules with adjacent sites (Uddin et al., 2017). The monolayer adsorption capacity (Q_0) of the DP is much higher than the IL-CNC@DP with values of 68 mg/g and 8.7 mg/g, respectively at 25 °C.

Table 3
Thermodynamic parameters for Li^+ adsorption onto IL-CNC@DP and DP.

Adsorbent	Temperature (°C)	ln (K_L)	ΔG° (kJ/mol)	ΔH° (kJ/mol)	ΔS° (kJ/mol.K)
IL-CNC@DP	25	4.46	-11.21	-74.57	-0.21
	35	3.67	-9.08		
	45	2.57	-6.96		
DP	25	5.14	-12.25	-46.05	-0.11
	35	3.93	-11.11		
	45	3.98	-9.98		

Table 4
The parameters of the two isotherms models for lithium adsorption onto IL-CNC@DP and DP at 25 °C, 35 °C, and 45 °C.

Adsorbent	T (°C)	Langmuir			Freundlich			
IL-CNC@DP		Q_0 (mg/g)	b (L/mg)	R^2	K_f (mg/g) (L/g)^n	n	1/n	R^2
	25	8.7	86.7	0.94	114.9	0.19	5.0	0.97
	35	5.6	39.1	0.94	221.6	0.18	5.4	0.97
	45	3.09	13.0	0.96	203.0	0.20	4.8	0.96
	T (°C)	**Temkin**			**Dubinin-Radushkevich**			
		A_T (L/mg)	B (J/mol)	R^2	q_s (mg/g)	B_D	R^2	
	25	0.63	28.9	0.80	674.5	-9×10^{-7}	0.97	
	35	0.69	26.6	0.86	1098	-7×10^{-7}	0.98	
	45	0.46	4.5	0.96	808	-6×10^{-7}	0.92	
DP	**T (°C)**	**Langmuir**			**Freundlich**			
		Q_0 (mg/g)	b (L/mg)	R^2	K_f (mg/g) (L/g)^n	n	1/n	R^2
	25	68.0	170.4	0.83	128.8	0.14	6.8	0.94
	35	32.7	50.6	0.93	529.8	0.102	9.7	0.90
	45	34.7	53.7	0.92	336.2	0.106	9.3	0.95
	T (°C)	**Temkin**			**Dubinin-Radushkevich**			
		A_T (L/mg)	B (J/mol)	R^2	q_s (mg/g)	B_D	R^2	
	25	0.54	25.0	0.90	41.1	-0.0001	0.90	
	35	0.52	16.9	0.95	48.9	-8×10^{-5}	0.91	
	45	0.54	33.3	0.91	44.0	-8×10^{-5}	0.89	

Moreover, the b constant values indicate the adsorbent and adsorbate affinity offers the presence of strong binding of Li^+ onto both of the adsorbents (Al-Ghouti et al., 2019). Therefore, based on the Langmuir isotherm model the adsorption of Li^+ onto DP is more favorable than IL-CNC@DP. These results mean that the DP adsorbent best fits the Langmuir model theory. The R_L values of both adsorbents at all the studied temperatures were between values of 0 and 1, therefore this indicates an energetically favorable adsorption process (Zango et al., 2020). The Freundlich isotherm model also shows that the adsorption process of both adsorbents as they follow this model to great extent. The high R^2 values can conclude that the studied adsorbents are reversible and form non-uniform multilayers on the surface of the adsorbent (Vijayakumar et al., 2012). Moreover, the value of n of the IL-CNC@DP and DP corresponds to values that are less than 1. Therefore, both of the adsorption processes of Li^+ are considered unfavorable and chemical processes (Al-Ghouti & Al-Absi, 2020). Another important constant that is derived from this isotherm is 1/n. According to the results, the value is greater than 1 for both adsorbents, therefore this indicates a cooperative adsorption process. Moreover, the adsorption capacity of Li^+ of the adsorbents is represented by the Freundlich constant (K_f) (Zango et al., 2020). According to the obtained results, it is evident that both IL-CNC@DP and DP have high adsorption capacities at 114.9 mg/g and 128.8 mg/g at 25 °C, respectively, for Li^+ when referring to the Freundlich isotherm model. It can be concluded that both adsorbents fit this model. Another isotherm model, Dubinin–Radushkevich, has B_D values obtained for both adsorbents as shown in Table 2. The results demonstrate that the adsorption process of Li^+ is an energy-free process. In addition, the adsorption capacity (q_s) values of the isotherm model show that the IL-CNC@DP can attain higher adsorption of Li^+ than the DP at 25 °C. Furthermore, the R^2 values of IL-CNC@DP are higher than DP, which tends to provide a better description of the model than the DP for the adsorption of Li^+. Therefore, the Dubinin–Radushkevich isotherm model best fits the IL-CNC@DP.

The last isotherm model used in this study is the Temkin adsorption isotherm model. It is evident that the R^2 values indicate that the model gives great fitting to both types of adsorbents although with better fitting for the DP. As a result, the adsorption process of Li^+ depends on the heat of adsorption (Al-Ghouti & Al-Absi., 2020). The high values for the Temkin's heat of adsorption constant (B) will tend to offer a chemical exothermic adsorption process of Li^+ (de de de Farias Silva et al., 2020). It can be concluded that at 25 °C this model can fit both adsorbents.

The studies done at 35 °C and 45 °C for Langmuir, Freundlich, Dubinin–Radushkevich, and Temkin isotherm models are also demonstrated in Table 4. From Table 4, all the isotherm models for the two adsorbents show relatively high R^2 values at all temperatures, which means that the adsorption of Li^+ could follow all models. Yet, the IL-CNC@DP displayed the highest R^2 value with the Langmuir isotherm model at 45 °C, while with the Freundlich isotherm model, the highest R^2 is for IL-CNC@DP is at 35 °C. The Dubinin–Radushkevich isotherm model for IL-CNC@DP demonstrates the highest R^2 at 35 °C, whereas the Temkin isotherm model at 45 °C. The DP displayed the highest R^2 value with the Langmuir isotherm model at 35 °C, while with the Freundlich isotherm model; the highest R^2 for DP is at 45 °C. The highest R^2 values for the DP adsorbent with Dubinin–Radushkevich and Temkin isotherm model were observed at 35 °C. This signifies how the changes in temperature values impact the mechanism of adsorption onto the IL-CNC@DP and DP (Magdy et al., 2018). It is worth mentioning that the R^2 value reached 0.96 when the temperature increased to 45 °C for the IL-CNC@DP. This can indicate that that the adsorption of Li^+ onto IL-CNC@DP follows the Langmuir isotherm model better at higher temperatures, while the adsorption onto DP best fits the model at lower temperatures (35 °C). Although the monolayer adsorption capacity (Q_0) of both adsorbents at 35 and 45 °C did not drastically change as the temperature increased, however, the DP is much higher than the modified adsorbent regarding the adsorption capacity values. Moreover, the b constant values are more favorable towards DP based on the Langmuir isotherm model. As for the Freundlich isotherm model, as previously mentioned, the high R^2 values for the IL-CNC@DP and DP at

both temperatures (35 °C and 45 °C) show the fitting of the adsorption mechanism of Li^+. This means that Li^+ forms reversible and non-uniform multilayers on the surface of the adsorbent. Additionally, the value of n of the IL-CNC@DP and DP corresponds to values that are less than 1. Therefore, both of the adsorption processes of Li^+ are considered unfavorable and chemical processes at 35 °C and 45 °C. Regarding the modified adsorbent, the value of n at 45 °C is 0.20 and at 35 °C is 0.18; this indicates that the increased favorability of the adsorption occurs as the temperature increases to 45 °C. In addition, the constant 1/n for IL-CNC@DP is greater than 1, but it decreases as the temperature increases, which indicates a cooperative adsorption process as it becomes more heterogeneous. The Freundlich constant (K_f) for IL-CNC@DP did not significantly change when the temperature increased from 35 °C to 45 °C, meaning that they share comparable adsorption capacity towards Li^+. However, the K_f value of the DP decreased from 529.8 mg/g to 336.2 mg/g when the temperature increased from 35 °C to 45 °C, indicating the significant impact the temperature has on the adsorption capacity of DP. As for the Dubinin–Radushkevich isotherm model, the B_D results demonstrate that the adsorption process of Li^+ is an energy-free process and the adsorption capacity (q_s) values of the isotherm model show that the IL-CNC@DP at 35 °C displayed a higher adsorption capacity at 1098 mg/g than the DP at 529.8 mg/g for the removal of Li^+. Similar results demonstrate that at 45 °C, the IL-CNC@DP displayed a higher adsorption capacity at 808 mg/g than the DP at 336.2 mg/g. Lastly, the Temkin adsorption isotherm model R^2 values indicate that the model gives great fitting to both types of adsorbents although with better fitting for the DP at 35 & 45 °C. Moreover, positive values of Temkin's heat of sorption constant (B) offer a chemical exothermic adsorption process of Li^+ at both temperatures.

3.9. Desorption study of lithium

An important feature for any adsorbent material is its reusability because it determines the cost of treatment. In other words, if the adsorbent can be reused multiple times, thus the cost of treatment per unit volume of treated water is lower (Khan and Lo, 2016). Moreover, reusability considers three critical parameters: desorption, recovery, and stability of the adsorbent. The process of desorption is the complete opposite of adsorption since it involves the release of the adsorbed substances from their surface. Therefore, providing adsorption sites, where the adsorbent can be regenerated and reused again (Badsha et al., 2020). In this study, the main objective is to investigate the desorption process by using 0.5 M and 1 M HCl as eluents since it has been used for the desorption of Li^+ from spent IL-CNC@DP and DP. Hydrochloric acid was selected as a desorption agent to prevent the introduction of other anions in the medium (Lemaire et al., 2014). Table 5 demonstrates the percentage desorption for Li^+ using 0.5 M and 1 M HCl. The desorption calculation was performed as per Eq. (4).

From Table 5, it is evident that all the adsorbents achieved a desorption percentage of 99% and higher under both concentrations. This proves that the desorption process was not influenced by different HCl concentrations. It is further supported by the analysis of variance (ANOVA) test that was used to assess the significance between the two concentrations. A single-factor ANOVA test was conducted to study the effect of using 0.5 M and 1 M HCl for each adsorbent. The results show that no significant difference was found at a p-value of 0.16. Furthermore, the high desorption efficiency suggests that the adsorption mechanism of Li^+ onto IL-CNC@DP and DP was mainly a physical adsorption process and that the binding was weak (Badsha et al., 2020; Carvalho et al., 2020). In the end, both adsorbents can be regenerated and reused, making them economically feasible and environmentally friendly (Kyzas and Kostoglou, 2014). Furthermore, recovery of Li^+ for other applications can be employed.

In conclusion, the finding of this study proves that Li^+ had high desorption efficiencies for both adsorbents at two different concentrations, therefore, the spent adsorbent of Li^+ can be reused for future adsorption processes and the recovery of Li^+ can occur. Bearing in mind that it also demonstrates exceptional adsorptive capacities as mentioned previously in the study.

3.10. Application of DP and IL-CNC@DP to a real groundwater sample

The adsorption of specific metals on an adsorbent is typically influenced by the presence of other ions in the solution. This is due to the competition that might occur between the ions onto the adsorbents' binding sites (Naeimi and Faghihian, 2017). Most research papers refer to it as the selectivity of targeted ions towards an adsorbent with the presence of other background ions. Moreover, high selectivity is necessary for any adsorptive treatment specifically towards heavy metals, whose remediation from the environment is a major concern (Badsha et al., 2020). Therefore, investigating the selectivity of metal adsorption is very critical since higher selectivity tends to make the most of the active sites of the adsorbent, while simultaneously recovering metals from the solution.

In this study, groundwater (GW) samples were obtained from the northern wells to evaluate Qatar's groundwater quality (Ahmad et al., 2020). Hence, a multi-element analysis of the groundwater sample was performed, and the results are illustrated in Table 6. It was important to investigate the adsorption selectivity of the modified IL-CNC@DP and DP between those co-existed cations and Li^+. It can be seen that twelve elements were detected by the ICP-OES and that in general the IL-CNC@DP and DP are not selective only towards the studied metal. For example, Sr, Mg, and Ga concentrations after the addition of IL-CNC@DP decreased slightly in comparison to DP. This suggests that IL-CNC@DP can be used to treat other cations better than DP implying that the adsorbent is capable of working effectively even in a matrix of various ions. On the other hand, some cations in the groundwater are not properly adsorbed by the IL-CNC@DP and they remained unchanged once the unmodified adsorbent was added. For example, Ca was found to be 643 mg/L in the groundwater sample even after the addition of the DP, whereas the concentration slightly changed after the addition of the IL-CNC@DP to 641 mg/L. This implies that only the IL-CNC@DP can be effective towards Ca. Furthermore, K and In concentrations remained unchanged after the addition of the IL-CNC@DP, whereas the concentration slightly changed after the addition of the IL-CNC@DP. As for Na, it is the highest ion detected in the groundwater sample at 4526 mg/L. After the adsorption by IL-CNC@DP, the concentration of Na dropped to 4208 mg/L. This result is significant since the IL-CNC@DP is effective towards large quantities of Na ions. Furthermore, after the adsorption by DP, the concentration also dropped to 4459 mg/L, implying that the DP can be employed towards Na. Besides, Al cation is slightly effective towards DP than IL-CNC@DP in the presence of other ions, whereas Ba cation did not significantly change after the addition of both adsorbents. In the end, this depends upon the different mechanisms of adsorption of

Table 5
Effect of different eluent concentrations on Li^+ desorption efficiency (%) onto IL-CNC@DP and DP.

Adsorbent	Eluent concentration	Average adsorbed concentration (mg/L)	Desorption (%)
IL-CNC@DP	0.5 M HCl	35.27	99.920
	1 M HCl		99.994
DP	0.5 M HCl	14.44	99.923
	1 M HCl		99.993

Table 6
Multi-element analysis for groundwater sample before and after adsorption by IL-CNC@DP and DP. Experimental conditions: particle size: 0.125–0.250 mm, adsorbent mass: 0.05 g, temperature: 25 °C, groundwater volume: 50 mL, and contact time: 24 h.

	Al	Ba	Mo	Sr	B	Li	Ca	Mg	Na	K	Ga	In
	Concentration (mg/L)											
Initial GW composition	0.039	0.018	0.05	13.72	1.760	0.255	643	229	4526	125	0.231	0.009
IL-CNC@DP	0.039	0.017	0.01	13.13	1.701	0.246	641	224	4208	124	0.135	0.008
DP	0.037	0.017	0.02	13.67	1.743	0.250	643	228	4459	125	0.161	0.009

each metal according to their physicochemical properties. As for Li^+ the concentration, 0.255 mg/L after the adsorption by the IL-CNC@DP, decreased slightly to 0.246 mg/L, were in comparison with the DP, it remained higher at 0.250 mg/L. It is clear that the presence of other ions in the groundwater samples is influenced by the addition of both adsorbents. Moreover, the differences between the concentrations of IL-CNC@DP and DP in comparison to the groundwater sample are not that significant. This means that the availability of other ions in the groundwater sample compete with Li^+ for the active sites onto both adsorbents. This can also decrease the adsorption efficiency and capacity of Li^+ if other ions are found in the solution. Nonetheless, the following section provides an idea regarding the adsorption mechanism and the reason behind the selectivity of the ions towards the adsorbents.

3.11. Mechanisms of adsorption onto IL-CNC@DP modified adsorbent

The adsorption mechanisms of Li^+ onto IL-CNC@DP and DP surface could be affected by various factors. One of these factors is the solubility of the Li^+ ions relative to the solvent. Moreover, it could be due to the affinity the Li^+ possesses towards the adsorbent. Therefore, this type of attraction could be mainly due to electrical, van der Waals forces, or chemical reactions. The surface of the adsorbent and its outcome on the process of adsorption is significant to understand the entire Li^+ adsorption. The FTIR results can help determine the relationship and interaction between the Li^+ and functional groups that are found on the surface of the adsorbent. Other parameters such as the effect of pH and initial Li^+ concentration are of importance in determining the adsorption mechanisms. However, multiple adsorption mechanisms such as electrostatic attractions, chelation, ion exchange, bridging, π-π interactions, hydrogen bonding, and complexation could also be employed in the adsorption mechanisms (Zhang et al., 2019). This work investigates the adsorption mechanisms of Li^+ from aqueous solutions onto the novel IL-CNC@DP.

The uptake of Li^+ from aqueous solutions is significantly influenced by the chemistry and surface morphology of the adsorbent. It is worth mentioning that the DP is considered acidic in nature with a pH value of 4.6 (Al-Ghouti et al., 2010). This is because of the presence of multiple functional groups such as phenolic hydroxides, alcohols, and ethers. Furthermore, under acidic conditions, when the pH is too low, the functionality of the groups is not changed, whereas, at higher pH values, the groups will begin to neutralize their activities and binding properties (Al-Ghouti et al., 2010). The DP is mainly composed of cellulose with the

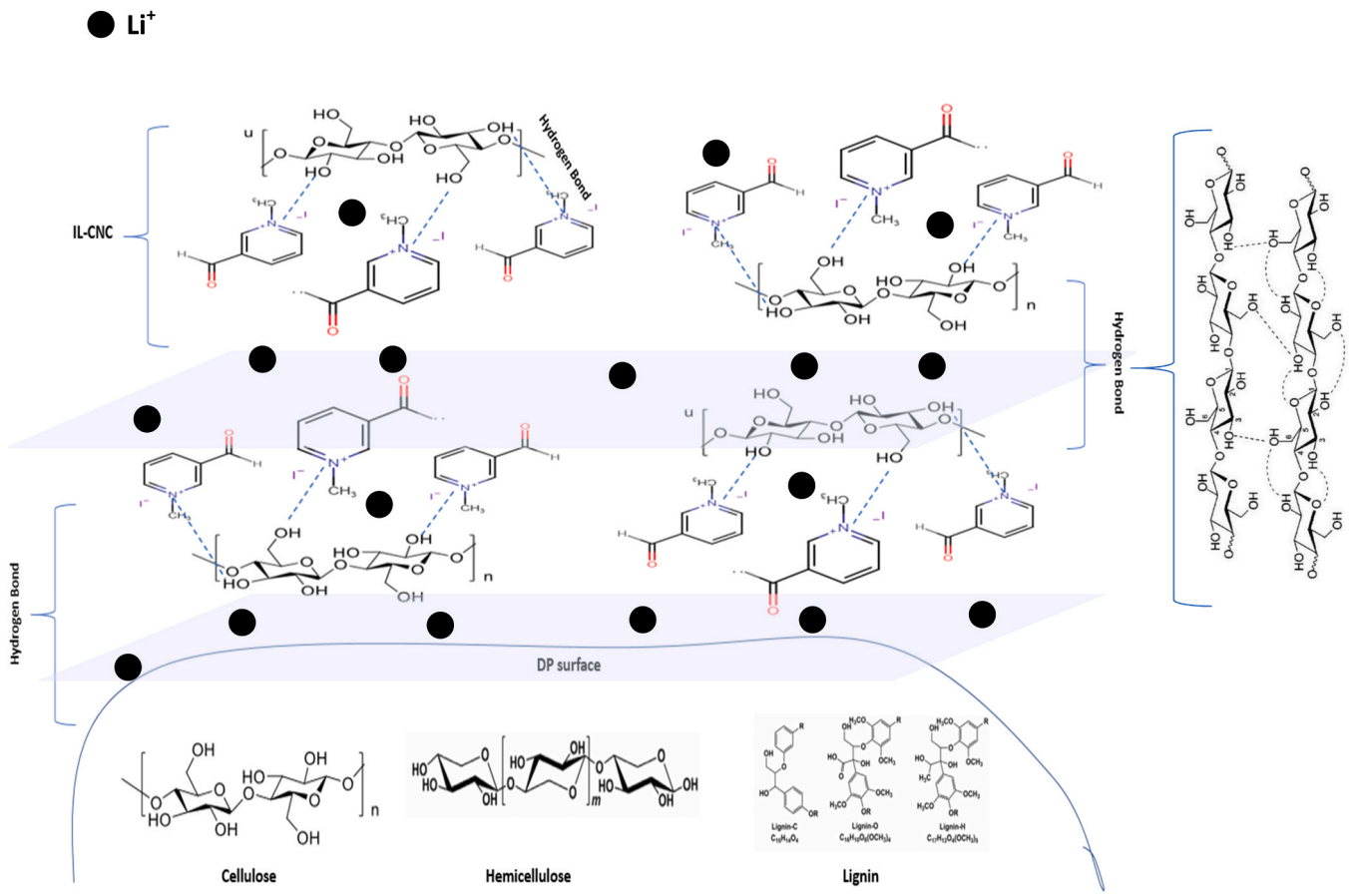

Fig. 10. Schematic representation of the IL-CNC@DP and proposed different Li^+ adsorption mechanisms onto the IL-CNC@DP.

empirical formula of $(C_6H_{10}O_5)_n$. In addition, 28.1% and 19.9% account for hemicellulose and lignin, respectively (Al-Ghouti et al., 2019). In Fig. 10, it can be seen that the DP consists of mainly cellulose, hemicellulose, and lignin (Díez et al., 2020). Cellulose and hemicellulose comprise the majority of oxygen functional groups such as hydroxyl, ether, and carbonyl that are found in the lignocellulosic components of DP. On the other hand, lignin is considered a complex polymer of aromatic substances, which tends to act as a cementing matrix that binds within and amongst cellulose and hemicellulose components (Lu et al., 2017). Therefore, the existence of these groups on the surface of the adsorbent considerably influences the adsorption characteristics of Li^+. Hydrogen bonding and electrostatic interactions are conserved as the dominant adsorption mechanisms due to the hydroxyl groups of cellulose, hemicellulose, and lignin and the oxygen atom of the aldehyde compound that is found in the IL.

It is worth mentioning that the DP used throughout this whole study had two main roles. Firstly, cellulose is extracted from the DP and then converted to CNCs to have a high surface-to-volume ratio. Secondly, the DP is used as a supporting material, where it can facilitate the adsorption process by forming a film layer over its surface with IL-CNC that promotes high surface to volume ratio, biodegradability, high functionalizability, and sustainability. Also, the fact that the percentage removal efficiency was dependent on the pH value; therefore this can indicate that ion exchange and electrostatic interactions are involved in the removal of the Li^+ ion by IL-CNC@DP and DP. The availability of hydroxyl groups, as previously mentioned, would help in the adsorption process, which will enhance the adsorbent binding levels along with the electrostatic interactions that are occurring. The mechanism of ion exchange occurs as Li^+ ions bind to the anionic sites by returning protons from acidic groups found on the adsorbent's surface (Hawari et al., 2014). The adsorption behavior of Li^+ ions onto the IL-CNC@DP surface might be explained by the fact that when ions are added, the ions willingly adsorb on the surface of the adsorbent. This action at first initially happens on the external surface of the adsorbent, therefore high Li^+ concentrations will tend to increase. In addition, monodentate aggregates of Li^+ exclusively occur onto the adsorbent. This means that depending upon the size and orientation of adsorbed Li^+ ions different structural surface complexes tend to form, as shown in Fig. 10. It is important to mention that there is a chance these ions migrate and penetrate from the external surface of the adsorbent to their pores (Hawari et al., 2014).

However, it is important to note that the reason why the selectivity of some ions is more than others relies on the characteristic properties of the ions such as their crystal radius, equilibrium constant, and electronegativity. In this study, the size and structure of each ion tend to impact the mechanism and the mobility of the ions such as the crystal radius. In general, ions with larger electronegativity and high hydrolysis coefficients, adsorb effortlessly. On the other hand, ions with high ionic radius have low charge density and low electrostatic attraction. This will tend to decrease the adsorption (Minceva et al., 2008). In other words, Li^+ has a crystal radius value of 0.9 Å (Shannon, 1976). Therefore, the adsorption occurs on the surface of the modified adsorbent (inter-particle diffusion) and migrates into the pores of the adsorbents (intra--particle diffusion) since it has a small crystal radius value (Hawari et al., 2014). Moreover, the adsorption mechanisms can be studied according to the ion hydrolysis constant (pKa), where a larger hydrolysis constant would increase the adsorptive capacity. It is evident that Li^+ reacts to give a feebly acidic cation like Li(OH) with a pKa value of 13.6 (Miessler et al., 2014). According to the obtained results of the effect of initial concentration and temperature, the adsorption capacity of Li^+ reached 99 mg/g at 100 mg/L of initial ion concentration onto IL-CNC@DP. Therefore, this is why the adsorptive capacity of Li^+ is quite high in the batch adoption tests. On the other hand, comparing the obtained real groundwater results of Li^+ with Na^+, it can be concluded that Na^+ presented better results after the addition of the adsorbents. This implies that the IL-CNC@DP adsorbent is effective towards large quantities of Na^+ ions. Furthermore, Na^+ has a crystal radius of 1.16, which is quite high in comparison to Li^+ crystal radius, however, its equilibrium constant and electronegativity values of 15.7 and 0.93, respectively, validates the reason why the adsorption ability of Na^+ in real groundwater is high in comparison to Li^+ adsorption (Miessler et al., 2014; Wulfsberg, 1991). In addition, the ion's adsorption mechanism can be discussed according to the electronegativity of each ion. This means that the metal with the highest electronegativity tends to adsorb more easily. However, Li^+ and Na^+ have almost the same electronegativity at 0.91 and 0.93, respectively, but different adsorption results in the real groundwater system (Wulfsberg, 1991). This might explain our above hypothesis that the inter- and intra-particle diffusion is the controlling mechanism of adsorption in the case of Li^+ and that the adsorption of Na^+ occurs most probably only onto the external surface of the adsorbent (inter-particle diffusion) due to its high crystal radius value. Furthermore, this implies why their adsorption after the adsorbents are added are different from one another in the real groundwater. Also, for example, comparing Ga^{3+} adsorption versus Li^+ adsorption, we can conclude it presented better results in the groundwater study. This could also be due to the crystal radius (0.76) and electronegativity (1.81) values that make it inclined to be adsorbed more than Li^+ (Wulfsberg, 1991; Shannon, 1976). In the end, we can conclude that future production of adsorbents towards selectivity of specific elements is in fact influenced by its physicochemical characteristics, and modifying a novel adsorbent further for the optimum selective adsorption of lithium is still required especially in a matrix of highly polluted systems with elements that exceed the permissible limits.

4. Conclusion

This study is considered the first of its kind as it demonstrated a modified novel adsorbent (IL-CNC@DP). CNCs have been successfully isolated from DP by sulfuric acid hydrolysis. Furthermore, this adsorbent can be used to treat Li^+ contamination in aqueous solutions by making use of agricultural wastes such as date pits. The preparation of the adsorbent is cost-effective and environmentally friendly. According to the results, Li^+ ions can be effectively remediated at high percentage removal by using the modified adsorbent in comparison to DP. The effect of pH and initial concentration had an impact on the adsorption of the metal, while the effect of temperature did not impact the adsorption significantly. The results demonstrate that at 25 °C at an initial concentration of 100 mg/L, Li^+ reached 99 mg/g. Considering all parameters and temperatures, we can conclude that the highest adsorption capacity (q_e) was at 100 mg/L at pH 6 for IL-CNC@DP. Furthermore, the thermodynamics constants of the modified adsorbent proved that the adsorption process was exothermic, did not favor a high level of disorder, and is spontaneous in nature. Langmuir, Freundlich, Dubinin–Radushkevich, and Temkin isotherm models were successfully used to find the best-fit model and the results varied according to each adsorbent used. Moreover, desorption studies proved that Li^+ is capable of being desorbed under the two adsorbents. The selectivity of the IL-CNC@DP towards real groundwater samples isolated in Qatar depends upon the physicochemical characteristics of each element. Finally, characterization by SEM, BET, and FTIR proved that the IL-CNC@DP was improved due to the enhancement of its surface morphology, an increase of surface area, and the presence of functional groups. In this current study, IL-CNC@DP confirmed exceptional results proving that the modification enhanced the remediation of Li^+ from water.

CRediT authorship contribution statement

Sara A. Wahib: Methodology, Formal analysis, Validation, Investigation, Writing – review & editing. **Dana A. Da'na:** Methodology, Formal analysis, Validation, Investigation, Writing – review & editing. **Nabil Zaouri:** Methodology, Formal analysis, Validation, Investigation, Writing – review & editing. **Yousef M. Hijji:** Methodology, Formal

analysis, Validation, Investigation, Writing – review & editing. **Mohammad A. Al-Ghouti:** Conceptualization, Supervision, Visualization, Methodology, Formal analysis, Validation, Investigation, Writing – review & editing..

Declaration of Competing Interest

The authors declare that they have no known competing financial interests or personal relationships that could have appeared to influence the work reported in this paper.

Acknowledgment

This publication was made possible by NPRP grant # [12S-0307-190250] from the Qatar National Research Fund (a member of Qatar Foundation). The findings achieved herein are solely the responsibility of the author[s].

References

Abu-Thabit, N.Y., Judeh, A.A., Hakeem, A.S., Ul-Hamid, A., Umar, Y., Ahmad, A., 2020. . Isolation and characterization of microcrystalline cellulose from date seeds (Phoenix dactylifera L.). Int. J. Biol. Macromol. 155, 730–739.

Aguayo, M., Fernández Pérez, A., Reyes, G., Oviedo, C., Gacitúa, W., Gonzalez, R., Uyarte, O., 2018. Isolation and characterization of cellulose nanocrystals from rejected fibers originated in the kraft pulping process. Polymers 10 (10), 1145.

Ahmad, A.Y., Al-Ghouti, M.A., Khraisheh, M., Zouari, N., 2020. Hydrogeochemical characterization and quality evaluation of groundwater suitability for domestic and agricultural uses in the state of Qatar. Groundw. Sustain. Dev. 11, 100467.

Aldawsari, A., Khan, M.A., Hameed, B.H., Alqadami, A.A., Siddiqui, M.R., Alothman, Z. A., Ahmed, A.Y.B.H., 2017. Mercerized mesoporous date pit activated carbon—A novel adsorbent to sequester potentially toxic divalent heavy metals from water. PloS One 12 (9).

Al-Ghouti, M., Li, J., Salamh, Y., Al-Laqtah, N., Walker, G., Ahmad, M., 2010. Adsorption mechanisms of removing heavy metals and dyes from aqueous solution using date pits solid adsorbent. J. Hazard. Mater. 176 (1–3), 510–520. https://doi.org/10.1016/j.jhazmat.2009.11.059.

Al-Ghouti, M.A., Da'ana, D.A., 2020. Guidelines for the use and interpretation of adsorption isotherm models: A review. J. Hazard. Mater. 393, 122383.

Al-Ghouti, M.A., Al Disi, Z.A., Al-Kaabi, N., Khraisheh, M., 2017. Mechanistic insights into the remediation of bromide ions from desalinated water using roasted date pits. Chem. Eng. J. 308, 463–475.

Al-Ghouti, M.A., Da'ana, D., Abu-Dieyeh, M., Khraisheh, M., 2019. Adsorptive removal of mercury from water by adsorbents derived from date pits. Sci. Rep. 9 (1), 1–15.

Al-Ghouti, M.A., Al-Absi, R.S., 2020. Mechanistic understanding of the adsorption and thermodynamic aspects of cationic methylene blue dye onto cellulosic olive stones biomass from wastewater. Sci. Rep. 10 (1), 1–18.

Anantha, M.S., Olivera, S., Hu, C., Jayanna, B.K., Reddy, N., Venkatesh, K., Naidu, R., 2020. Comparison of the photocatalytic, adsorption and electrochemical methods for the removal of cationic dyes from aqueous solutions. Environ. Technol. Innov. 17, 100612.

Baalousha, H.M., Ouda, O.K., 2017. Domestic water demand challenges in Qatar. Arab. J. Geosci. 10 (24), 537.

Badsha, M.A., Khan, M., Wu, B., Kumar, A., Lo, I.M., 2020. Role of surface functional groups of hydrogels in metal adsorption: from performance to mechanism. J. Hazard. Mater., 124463

Carvalho, T., Pereira, A.D.S., Bonomo, R.C., Franco, M., Finotelli, P.V., Amaral, P.F., 2020. Simple physical adsorption technique to immobilize Yarrowia lipolytica lipase purified by different methods on magnetic nanoparticles: adsorption isotherms and thermodynamic approach. Int. J. Biol. Macromol. 160, 889–902.

Chandra, J., George, N., Narayanankutty, S.K., 2016. Isolation and characterization of cellulose nanofibrils from arecanut husk fibre. Carbohydr. Polym. 142, 158–166.

Darwish, M.A., Mohtar, R., 2013. Qatar water challenges. Desalin. Water Treat. 51 (1–3), 75–86.

Díez, D., Urueña, A., Piñero, R., Barrio, A., Tamminen, T., 2020. Determination of hemicellulose, cellulose, and lignin content in different types of biomasses by thermogravimetric analysis and pseudocomponent kinetic model (TGA-PKM Method). Processes 8 (9), 1048.

Eggermont, S.G., Prato, R., Dominguez-Benetton, X., Fransaer, J., 2020. Metal removal from aqueous solutions: insights from modeling precipitation titration curves. J. Environ. Chem. Eng. 8 (1), 103596.

Engwayu, J., Pawlik, M., 2020. Adsorption of anionic polymers on hematite–a study of zeta potential distributions. Mineral. Eng. 148, 106225.

Fakhfakh, J., Ben-Youssef, S., Naushad, M., Allouche, N., 2019. Different extraction methods, physical properties and chemical composition of date seed oil. In: Int. Sustainable Agriculture Reviews, 34. Springer,, Cham, pp. 125–153.

de Farias Silva, C.E., da Gama, B.M.V., da Silva Gonçalves, A.H., Medeiros, J.A., de Souza Abud, A.K., 2020. Basic-dye adsorption in albedo residue: effect of pH, contact time, temperature, dye concentration, biomass dosage, rotation and ionic strength. J. King Saud. Univ. Eng. Sci. 32 (6), 351–359.

Gholami-Bonabi, L., Ziaefar, N., Sheikhloie, H., 2020. Removal of phenol from aqueous solutions by magnetic oxide graphene nanoparticles modified with ionic liquids using the Taguchi optimization approach. Water Sci. Technol. 81 (2), 228–240.

Girish, C.R., Murty, V.R., 2016. Mass transfer studies on adsorption of phenol from wastewater using Lantana camara, forest waste. Int. J. Chem. Eng. 2016.

Guo, Y., Zhang, Y., Zheng, D., Li, M., Yue, J., 2020. Isolation and characterization of nanocellulose crystals via acid hydrolysis from agricultural waste-tea stalk. Int. J. Biol. Macromol. 163, 927–933.

Hawari, A., Khraisheh, M., Al-Ghouti, M.A., 2014. Characteristics of olive mill solid residue and its application in remediation of Pb2+, Cu2+ and Ni2+ from aqueous solution: mechanistic study. Chem. Eng. J. 251, 329–336.

Heibati, B., Rodriguez-Couto, S., Amrane, A., Rafatullah, M., Hawari, A., Al-Ghouti, M. A., 2014. Uptake of Reactive Black 5 by pumice and walnut activated carbon: chemistry and adsorption mechanisms. Ind. Eng. Chem. Res. 20 (5), 2939–2947.

Hilal, N.M., Ahmed, I.A., El-Sayed, R.E., 2012. Activated and nonactivated date pits adsorbents for the removal of copper (II) and cadmium (II) from aqueous solutions. Phys. Chem. 2012.

Hussein, H., Lambert, L.A., 2020. A rentier state under blockade: qatar's water-energy-food predicament from energy abundance and food insecurity to a silent water crisis. Water J. 12 (4), 1051.

Imran Din, M., Mirza, M.L., Ata, S., Athar, M., Mohsin, I.U., 2013. Thermodynamics of biosorption for removal of Co (II) ions by an efficient and ecofriendly biosorbent (Saccharum bengalense): kinetics and isotherm modeling. J. Chem. 2013.

Irfan, M., Ahmad, T., Moniruzzaman, M., Bhattacharjee, S., Abdullah, B., 2020. Size and stability modulation of ionic liquid functionalized gold nanoparticles synthesized using Elaeis guineensis (oil palm) kernel extract. Arab. J. Chem. 13 (1), 75–85.

Ismail, H., 2015. Food and Water Security in Qatar: Part 2–Water Resources. Future Directions International Pty Ltd, Dalkeith WA, Australia.

Jiang, N., Shang, R., Heijman, S.G., Rietveld, L.C., 2020. Adsorption of triclosan, trichlorophenol and phenol by high-silica zeolites: adsorption efficiencies and mechanisms. Sep. Purif. Technol. 235, 116152.

Kamran, U., Park, S.J., 2020. Functionalized titanate nanotubes for efficient lithium adsorption and recovery from aqueous mediaJ. Solid State Chem. 283, 121157.

Kamran, U., Heo, Y.J., Lee, J.W., Park, S.J., 2019. Chemically modified activated carbon decorated with MnO2 nanocomposites for improving lithium adsorption and recovery from aqueous media. J. Alloy. Compd. 794, 425–434.

Khalil, H., Alqahtani, N., Darrag, H., Ibrahim, H., Emeka, P., Badger-Emeka, L., et al., 2021. Date palm extract (Phoenix dactylifera) PEGylated nanoemulsion: development, optimization and cytotoxicity evaluation. Plants 10 (4), 735.

Khan, M., Lo, I.M., 2016. A holistic review of hydrogel applications in the adsorptive removal of aqueous pollutants: recent progress, challenges, and perspectives. Water Res 106, 259–271.

Kyzas, G.Z., Kostoglou, M., 2014. Green adsorbents for wastewaters: a critical review. Materials 7 (1), 333–364.

Lemaire, J., Svecova, L., Lagallarde, F., Laucournet, R., Thivel, P., 2014. Lithium recovery from aqueous solution by sorption/desorption. Hydrometallurgy 143, 1–11.

Li, Z., Taubert, A., 2009. Cellulose/gold nanocrystal hybrids via an ionic liquid/aqueous precipitation route. Molecules 14 (11), 4682–4688.

Liang, S., Cao, S., Liu, C., Zeb, S., Cui, Y., Sun, G., 2020. Heavy metal adsorption using structurally preorganized adsorbent. RSC Adv. 10 (12), 7259–7264.

Lu, Y., Lu, Y.C., Hu, H.Q., Xie, F.J., Wei, X.Y., Fan, X., 2017. Structural characterization of lignin and its degradation products with spectroscopic methods. J. Spectrosc. 2017.

Magdy, Y.M., Altaher, H., ElQada, E., 2018. Removal of three nitrophenols from aqueous solutions by adsorption onto char ash: equilibrium and kinetic modeling. Appl. Water Sci. 8 (1), 1–15.

Mahfoudhi, N., Boufi, S., 2017. Nanocellulose as a novel nanostructured adsorbent for environmental remediation: a review. Cellulose 24 (3), 1171–1197.

Manirethan, V., Gupta, N., Balakrishnan, R.M., Raval, K., 2019. Batch and continuous studies on the removal of heavy metals from aqueous solution using biosynthesised melanin-coated PVDF membranes. Environ. Sci. Pollut. 1–15.

Marett, J., Aning, A., Foster, E.J., 2017. The isolation of cellulose nanocrystals from pistachio shells via acid hydrolysis. Ind. Crop. Prod. 109, 869–874.

Mathew, B.T., Raji, S., Dagher, S., Hilal-Alnaqbi, A., Mourad, A.H.I., Al-Zuhair, S., Amin, A., 2018. Bilirubin detoxification using different phytomaterials: characterization and in vitro studies. Int J. Nanomed. 13, 2997.

Miessler, G.L., Fischer, P.J., Tarr, D.A., 2014. Inorganic Chemistry, 5th ed. Pearson, Boston, MA, USA, p. 2014.

Minceva, M., Fajgar, R., Markovska, L., Meshko, V., 2008. Comparative Study of Zn2 , Cd2 , and Pb2 Removal From Water Solution Using Natural Clinoptilolitic Zeolite and Commercial Granulated Activated Carbon. Equilibrium of Adsorption. Sep. Sci. Technol. 43 (8), 2117–2143. https://doi.org/10.1080/01496390801941174.

Morais, J.P., Rosa, M.D.F., Moreira de Souza, M.D.S., Nascimento, L.D., Nascimento, D. M., Cassales, A.R., 2013. Extraction and characterization of nanocellulose structures from raw cotton linter. Carbohydr. Polym. 91, 229–235.

Morán, J.I., Alvarez, V.A., Cyras, V.P., Vázquez, A., 2008. Extraction of cellulose and preparation of nanocellulose from sisal fibers. Cellulose 15 (1), 149–159.

Naeimi, S., Faghihian, H., 2017. Performance of novel adsorbent prepared by magnetic metal-organic framework (MOF) modified by potassium nickel hexacyanoferrate for removal of Cs+ from aqueous solution. Sep. Purif. Technol. 175, 255–265.

Nizam, N.U.M., Hanafiah, M.M., Mahmoudi, E., et al., 2021. The removal of anionic and cationic dyes from an aqueous solution using biomass-based activated carbon. Sci. Rep. 11, 8623.

Palomar, J., Lemus, J., Gilarranz, M.A., Rodriguez, J.J., 2009. Adsorption of ionic liquids from aqueous effluents by activated carbon. Carbon 47 (7), 1846–1856.

Pyrzynska, K., 2019. Removal of cadmium from wastewaters with low-cost adsorbents. J. Environ. Chem. Eng. 7, 102795.
Samra, S.E., Jeragh, B., EL-Nokrashy, A.M., El-Asmy, A.A., 2014. Biosorption of Pb2+ from natural water using date pits: a green chemistry approach Mod. Chem. A.
Shannon, R.D., 1976. Revised effective ionic radii and systematic studies of interatomic distances in halides and chalcogenides. Acta Crystallogr. Sect. A Cryst. Phys. Diffr. Theor. Gen. Crystallogr. 32 (5), 751–767.
Shi, T., Ma, J., Wu, X., Wu, F., 2018. Inventories of heavy metal inputs and outputs to and from agricultural soils: A review. Ecotoxicol. Environ. Saf. 164, 118–124.
Singh, H., Du, J., Singh, P., et al., 2018. Role of green silver nanoparticles synthesized from *Symphytum officinale* leaf extract in protection against UVB-induced photoaging. J. Nanostruct. Chem. 8, 359–368.
Tao, J., Yang, J., Ma, C., Li, J., Du, K., Wei, Z., Deng, X., 2020. Cellulose nanocrystals/graphene oxide composite for the adsorption and removal of levofloxacin hydrochloride antibiotic from aqueous solution. R. Soc. Open Sci. 7 (10), 200857.
Tian, L., Ma, W., Han, M., 2010. Adsorption behavior of Li+ onto nano-lithium ion sieve from hybrid magnesium/lithium manganese oxide. Chem. Eng. J. 156 (1), 134–140.
Trache, D., Hussin, M.H., Chuin, C.T.H., Sabar, S., Fazita, M.N., Taiwo, O.F., Haafiz, M. M., 2016.). Microcrystalline cellulose: Isolation, characterization and bio-composites application—A review. Int. J. Biol. Macromol. 93, 789–804.
Trilokesh, C., Uppuluri, K.B., 2019. Isolation and characterization of cellulose nanocrystals from jackfruit peel. Sci. Rep. 9 (1), 1–8.
Uddin, M.T., Rahman, M.A., Rukanuzzaman, M., Islam, M.A., 2017. A potential low cost adsorbent for the removal of cationic dyes from aqueous solutions. Appl. Water Sci. 7 (6), 2831–2842.
Verma, C., Mishra, A., Chauhan, S., Verma, P., Srivastava, V., Quraishi, M.A., Ebenso, E. E., 2019. Dissolution of cellulose in ionic liquids and their mixed cosolvents: a review. Sustain. Chem. Pharm. 13, 100162.
Vijayakumar, G., Tamilarasan, R., Dharmendirakumar, M., 2012. Adsorption, kinetic, equilibrium and thermodynamic studies on the removal of basic dye Rhodamine-B from aqueous solution by the use of natural adsorbent perlite. J. Mater. Environ. Sci. 3 (1), 157–170.
Wallace, D.R., Djordjevic, A.B., 2020. Heavy metal and pesticide exposure: a mixture of potential toxicity and carcinogenicity. Curr. Opin. Toxicol. 19, 72–79.
Wiśniewska, M., Fijałkowska, G., Ostolska, I., Franus, W., Nosal-Wiercińska, A., Tomaszewska, B., Wójcik, G., 2018a.). Investigations of the possibility of lithium acquisition from geothermal water using natural and synthetic zeolites applying poly (acrylic acid). J. Clean. Prod. 195, 821–830.
Wiśniewska, M., Fijałkowska, G., Ostolska, I., Franus, W., Nosal-Wiercińska, A., Tomaszewska, B., et al., 2018b. Investigations of the possibility of lithium acquisition from geothermal water using natural and synthetic zeolites applying poly (acrylic acid). J. Clean. Prod. 195, 821–830.
Wiśniewska, M., Franus, W., Fijałkowska, G., Ostolska, I., Wójcik, G., Nosal-Wiercińska, A., Goscianska, J., 2020. Adsorption and electrokinetic studies of sodalite/lithium/poly(acrylic acid) aqueous system. Physicochem. Probl. Miner. Process. 56 (6), 158–166.
Wulfsberg, G., 1991. Principles of descriptive inorganic chemistry. University Science Books.
Xiao, J., Nie, X., Sun, S., Song, X., Li, P., Yu, J., 2015a. Lithium ion adsorption–desorption properties on spinel Li4Mn5O12 and pH-dependent ion-exchange model. Adv. Powder Technol. 26 (2), 589–594.
Xiao, J., Nie, X., Sun, S., Song, X., Li, P., Yu, J., 2015b. Lithium ion adsorption–desorption properties on spinel Li4Mn5O12 and pH-dependent ion-exchange model. Adv. Powder Technol. 26 (2), 589–594.
Xu, C., Yu, T., Peng, J., Zhao, L., Li, J., Zhai, M., 2020. Efficient adsorption performance of lithium ion onto cellulose microspheres with sulfonic acid groups. Quantum Beam Sci. 4 (1), 6.
Yongvanich, N., 2015. Isolation of nanocellulose from pomelo fruit fibers by chemical treatments. J. Nat. Fibers 12, 323–331.
Yuan, C., Zhang, L., Li, H., Guo, R., Zhao, M., Yang, L., 2019. Highly selective lithium ion adsorbents: polymeric porous microsphere with crown ether groups. Trans. Tianjin Univ. 25 (2), 101–109.
Zango, Z.U., Bakar, N.H.H.A., Sambudi, N.S., Jumbri, K., Abdullah, N.A.F., Kadir, E.A., Saad, B., 2020. Adsorption of chrysene in aqueous solution onto MIL-88 (Fe) and NH2-MIL-88 (Fe) metal-organic frameworks: Kinetics, isotherms, thermodynamics and docking simulation studies. J. Environ. Chem. Eng. 8 (2), 103544.
Zante, G., Boltoeva, M., Masmoudi, A., Barillon, R., Trébouet, D., 2019. Lithium extraction from complex aqueous solutions using supported ionic liquid membranes. J. Membr. Sci. 580 (2019), 62–76.
Zhang, Q.H., Li, S.P., Sun, S.Y., Yin, X.S., Yu, J.G., 2010. LiMn2O4 spinel direct synthesis and lithium ion selective adsorption. Chem. Eng. Sci. 65 (1), 169–173.
Zheng, D., Zhang, Y., Guo, Y., Yue, J., 2019. Isolation and characterization of nanocellulose with a novel shape from walnut (Juglans regia L.) shell agricultural waste. Polym. J. 11 (7), 1130.
Zhong, J., Lin, S., Yu, J., 2021. Li+ adsorption performance and mechanism using lithium/aluminum layered double hydroxides in low grade brines. Desalination 505, 114983.
Zhuang, J., Li, M., Pu, Y., Ragauskas, A.J., Yoo, C.G., 2020. Observation of potential contaminants in processed biomass using fourier transform infrared spectroscopy. Appl 10 (12), 4345.